

Gluon-gluon contributions to the production of continuum diphoton pairs at hadron colliders

P. M. Nadolsky,¹ C. Balázs,¹ E. L. Berger,¹ and C.-P. Yuan²

¹*High Energy Physics Division, Argonne National Laboratory, Argonne, IL 60439, USA*

²*Department of Physics and Astronomy,
Michigan State University, East Lansing, MI 48824, USA*

(Dated: January 31, 2007)

Abstract

We compute the contributions to continuum photon pair production at hadron colliders from processes initiated by gluon-gluon and gluon-quark scattering into two photons through a four-leg virtual quark loop. Complete two-loop cross sections in perturbative quantum chromodynamics are combined with contributions from soft parton radiation resummed to all orders in the strong coupling strength. The structure of the resummed cross section is examined in detail, including a new type of unintegrated parton distribution function affecting azimuthal angle distributions of photons in the pair's rest frame. As a result of this analysis, we predict diphoton transverse momentum distributions in gluon-gluon scattering in wide ranges of kinematic parameters at the Fermilab Tevatron and the CERN Large Hadron Collider.

PACS numbers: 12.15.Ji, 12.38 Cy, 13.85.Qk

I. INTRODUCTION

Advances in the computation of higher-order radiative contributions in perturbative quantum chromodynamics (pQCD) open opportunities to predict hadronic observables at an unprecedented level of precision. Full realization of this potential requires concurrent improvements in the methods for QCD factorization and resummation of logarithmic enhancements in hadronic cross sections in infrared kinematic regions. All-orders resummation of logarithmic corrections, such as the resummation of transverse momentum (Q_T) logarithms in Drell-Yan-like processes [1], is increasingly challenging in multi-loop calculations as a result of algebraic complexity and new types of logarithmic singularities associated with multi-particle matrix elements.

In this paper, we address new theoretical issues in Q_T resummation at two-loop accuracy. We focus on photon pair production, particularly on the gluon-gluon subprocess, $gg \rightarrow \gamma\gamma$, one of the important short-distance subprocesses that contribute to the inclusive reactions $p\bar{p} \rightarrow \gamma\gamma X$ at the Fermilab Tevatron and $pp \rightarrow \gamma\gamma X$ at the CERN Large Hadron Collider (LHC). This hadronic reaction is interesting in its own right, and it is relevant in searches for the Higgs boson h , where it constitutes an important QCD background to the $pp \rightarrow hX \rightarrow \gamma\gamma X$ production chain [2, 3, 4]. A reliable prediction of the cross section for $gg \rightarrow \gamma\gamma$ is needed for complete estimates of the $\gamma\gamma$ production cross sections, a task that we pursue in accompanying papers [5, 6].

The lowest-order contribution to the cross section for $gg \rightarrow \gamma\gamma$ arises from a $2 \rightarrow 2$ diagram of order $\mathcal{O}(\alpha^2\alpha_s^2)$ involving a 4-vertex virtual quark loop [Fig. 1(a)]. We evaluate all next-to-leading (NLO) contributions of order $\mathcal{O}(\alpha^2\alpha_s^3)$ to the $gg \rightarrow \gamma\gamma$ process shown in Figs. 1(b-e). An important new ingredient in this paper is the inclusion of the $gq \rightarrow \gamma\gamma q$ process, Fig. 1(d), a necessary component of the resummed NLO contribution. Our complete treatment of the NLO cross section represents an improvement over our original publication [7], in which the large- Q_T behavior of the gg subprocess was approximated, and the gq contribution was not included. Furthermore, we resum to next-to-next-to-leading logarithmic (NNLL) accuracy the large logarithmic terms of the form $\ln(Q_T^2/Q^2)$ in the limit when Q_T of the $\gamma\gamma$ pair is much smaller than its invariant mass Q . Our NNLL cross section includes the exact \mathcal{C} coefficients of order α_s for $gg + gq \rightarrow \gamma\gamma X$, and the functions \mathcal{A} and \mathcal{B} of orders α_s^3 and α_s^2 in all subprocesses, with these functions defined in Sec. II.

We begin in Sec. II with a summary of kinematics and our notation, and we outline the partonic subprocesses that contribute to $\gamma\gamma$ production. In this section, we also derive a matrix element for the $gq \rightarrow \gamma\gamma q$ process shown in Fig. 1(d), a subprocess whose contribution is required to obtain consistent resummed predictions for all values of Q_T . We obtain the $\mathcal{O}(\alpha^2\alpha_s^3)$ cross section for the $gq \rightarrow \gamma\gamma q$ process from the color-decomposed $q\bar{q}ggg$ amplitudes in Ref. [8].

The rich helicity structure of the $gg \rightarrow \gamma\gamma$ matrix element is addressed in Sec. III. The helicity dependence requires a new type of transverse-momentum dependent (TMD) parton distribution function (PDF) associated with the interference of amplitudes for initial-state gluons of opposite helicities. The existence of the helicity-flip TMD PDF modifies the azimuthal angle distributions of the final-state photons, an effect that could potentially be observed experimentally. By contrast, in vector boson production $p\bar{p}^{(\pm)} \rightarrow VX$ (with $V = \gamma^*, W, Z, \dots$), such helicity-flip contributions are suppressed as a result of the simple spin structure of the lowest-order $q\bar{q}V$ coupling. In this section, we establish the presence of helicity interference in the finite-order $2 \rightarrow 3$ cross sections by systematically deriving

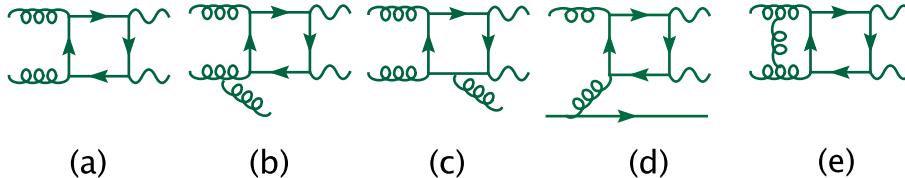


Figure 1: Representative parton scattering subprocesses for diphoton production in gluon-gluon scattering.

their soft and collinear limits in the splitting amplitude formalism [8, 9, 10, 11, 12, 13, 14]. We show how the helicity-flip TMD PDF arises from the general structure of the small- Q_T resummed cross section.

Section IV contains some numerical predictions for the Tevatron and LHC, where we show the fraction of the rate for $\gamma\gamma$ production supplied by the $gg + gq$ subprocess. The generally expected prominence of $gg + gq$ scattering at the LHC is only partially supported by our findings. The large gg partonic luminosity cannot fully compensate for the small cross section associated with gg scattering. Our findings are summarized in Sec. V. Three Appendices are included. In Appendix A, we present some of the details of our derivation of the amplitude for the subprocess $gg \rightarrow \gamma\gamma g$. In Appendix B, we derive the small- Q_T asymptotic form of the NLO cross section for $gg \rightarrow \gamma\gamma$.

II. NOTATION AND SUBPROCESSES

A. Notation

We consider the scattering process $h_1(P_1) + h_2(P_2) \rightarrow \gamma(P_3) + \gamma(P_4) + X$, where h_1 and h_2 are the initial-state hadrons. In terms of the center-of-mass collision energy \sqrt{S} , the $\gamma\gamma$ invariant mass Q , the $\gamma\gamma$ transverse momentum Q_T , and the $\gamma\gamma$ rapidity y , the momenta P_1^μ and P_2^μ of the initial hadrons and $q^\mu \equiv P_3^\mu + P_4^\mu$ of the pair are expressed in the laboratory frame as

$$P_1^\mu = \frac{\sqrt{S}}{2} \{1, 0, 0, 1\}; \quad (1)$$

$$P_2^\mu = \frac{\sqrt{S}}{2} \{1, 0, 0, -1\}; \quad (2)$$

$$q^\mu = \left\{ \sqrt{Q^2 + Q_T^2} \cosh y, Q_T, 0, \sqrt{Q^2 + Q_T^2} \sinh y \right\}. \quad (3)$$

The light-cone momentum fractions for the boosted $2 \rightarrow 2$ scattering system are

$$x_{1,2} \equiv \frac{2(P_{2,1} \cdot q)}{S} = \frac{\sqrt{Q^2 + Q_T^2} e^{\pm y}}{\sqrt{S}}. \quad (4)$$

Decay of the $\gamma\gamma$ pairs is described in the hadronic Collins-Soper frame [15]. The Collins-Soper frame is a rest frame of the $\gamma\gamma$ pair (with $q^\mu = \{Q, 0, 0, 0\}$ in this frame), chosen so that (a) the momenta \vec{P}_1 and \vec{P}_2 of the initial hadrons lie in the Oxz plane (with zero

azimuthal angle), and (b) the z axis bisects the angle between \vec{P}_1 and $-\vec{P}_2$. The photon momenta are antiparallel in the Collins-Soper frame:

$$P_3^\mu = \frac{Q}{2} \{0, \sin \theta_* \cos \varphi_*, \sin \theta_* \sin \varphi_*, \cos \theta_*\}, \quad (5)$$

$$P_4^\mu = \frac{Q}{2} \{0, -\sin \theta_* \cos \varphi_*, -\sin \theta_* \sin \varphi_*, -\cos \theta_*\}, \quad (6)$$

where θ_* and φ_* are the photon's polar and azimuthal angles. Our aim is to derive resummed predictions for the fully differential $\gamma\gamma$ cross section $d\sigma/(dQ^2 dy dQ_T^2 d\Omega_*)$, where $d\Omega_* = d\cos\theta_* d\varphi_*$ is a solid angle element around the direction of \vec{P}_3 in the Collins-Soper frame of reference defined in Eq. (5). The parton momenta and helicities are denoted by lowercase p_i and λ_i .

B. Scattering contributions

We concentrate on direct production of isolated photons in hard QCD scattering, the dominant production process at hadron colliders. A number of hard-scattering contributions to the processes $q\bar{q} + qq \rightarrow \gamma\gamma$, as well as photon production via fragmentation, have been studied in the past [16, 17, 18]. Our numerical calculations include the lowest-order process $q\bar{q} \rightarrow \gamma\gamma$ of order $\mathcal{O}(\alpha^2)$ and contributions from $q\bar{q} \rightarrow \gamma\gamma g$ and $(\bar{q})g \rightarrow \gamma\gamma(\bar{q})$ of order $\mathcal{O}(\alpha^2\alpha_s)$, where $\alpha(\mu) = e^2/4\pi$ and $\alpha_s(\mu) = g^2/4\pi$ are the running QED and QCD coupling strengths.

Glue-gluon scattering is the next leading direct production channel, with the full set of NLO contributions shown in Fig. 1. Production of $\gamma\gamma$ pairs via a box diagram in gg scattering as in Fig. 1(a) [19] is suppressed by two powers of α_s compared to the lowest-order $q\bar{q} \rightarrow \gamma\gamma$ contribution, but is enhanced by a product of two large gluon PDF's if typical momentum fractions x are small. The main $\mathcal{O}(\alpha^2\alpha_s^3)$, or NLO, corrections, include one-loop $gg \rightarrow \gamma\gamma g$ diagrams (b) and (c) derived in [20, 21], as well as 4-leg two-loop diagrams (e) computed in [22]. The real and virtual diagrams are combined in Ref. [23] to obtain the full NLO contribution from gg scattering. In this study we also include subleading NLO contributions from the process (d), $gq_S \rightarrow \gamma\gamma q_S$ via the quark loop, where $q_S = \sum_{i=u,d,s,\dots}(q_i + \bar{q}_i)$ denotes the flavor-singlet combination of quark scattering channels. The $gq_S \rightarrow \gamma\gamma q_S$ helicity amplitude is derived from the one-loop $q\bar{q}ggg$ amplitude [8] and explicitly presented in Appendix A. As a cross check, we verified that this amplitude correctly reproduces the known collinear limits. Our result does not confirm an expression for this amplitude available in the literature [24], which does not satisfy these limits. When evaluated in our resummation calculation under typical event selection conditions, $gg + gq_S$ scattering contributes about 20% and 10% of the total rate at the LHC and the Tevatron, respectively, but this fraction can be larger in specific regions of phase space.

III. THEORETICAL PRESENTATION

A. Small- Q_T asymptotics of the next-to-leading order cross section

When the transverse momentum Q_T of the diphoton approaches zero, the NLO production cross section $d\sigma/(dQ^2 dy dQ_T^2 d\Omega_*)$, or briefly $P(Q, Q_T, y, \Omega_*)$, is dominated by $\gamma\gamma$ recoil against soft and collinear QCD radiation. In this subsection we concentrate on the effects

of initial-state QCD radiation and derive the leading small- Q_T part of the NLO differential cross section, called the asymptotic term $A(Q, Q_T, y, \Omega_*)$.

The $\mathcal{O}(\alpha_s)$ asymptotic cross section valid at $Q_T^2 \ll Q^2$ consists of a few generalized functions that are integrable on an interval $0 \leq Q_T \leq P_T$, with P_T being a finite value of transverse momentum:

$$A(Q, Q_T, y, \Omega_*) = F_\delta(Q, y, \Omega_*)\delta(\vec{Q}_T) + F_1(Q, y, \Omega_*) \left[\frac{1}{Q_T^2} \ln \frac{Q^2}{Q_T^2} \right]_+ + F_0(Q, y, \Omega_*) \left[\frac{1}{Q_T^2} \right]_+ + \dots \quad (7)$$

The “+” prescription $[f(Q_T)]_+$ is defined for a function $f(Q_T)$ and a smooth function $g(Q_T)$ as

$$\int_0^{P_T^2} dQ_T^2 [f(Q_T)]_+ g(Q_T) \equiv \int_0^{P_T^2} dQ_T^2 f(Q_T) (g(Q_T) - g(0)); \quad (8)$$

$$[f(Q_T)]_+ = f(Q_T) \quad \text{for } Q_T \neq 0. \quad (9)$$

Subleading terms proportional to $(Q/Q_T)^p$ with $p \leq 1$ are neglected in Eq. (7). Its form is influenced by spin correlations between the initial-state partons and final-state photons. As a consequence of these spin correlations, the functions F_δ , F_0 , and F_1 depend on the direction of the final-state photons in the Collins-Soper frame (the polar angle θ_* and sometimes the azimuthal angle φ_*).

The spin dependence of the small- Q_T cross section in the $gg \rightarrow \gamma\gamma g$ and $gq_S \rightarrow \gamma\gamma q_S$ channels is complex. The Born-level process $g(p_1, \lambda_1) + g(p_2, \lambda_2) \rightarrow \gamma(p_3, \lambda_3) + \gamma(p_4, \lambda_4)$ is described by 16 non-zero helicity amplitudes $\mathcal{M}_4(p_1, \lambda_1; p_2, \lambda_2; p_3, \lambda_3; p_4, \lambda_4) \equiv \mathcal{M}_4(\lambda_1, \lambda_2, \lambda_3, \lambda_4)$ for quark-box diagrams of the type shown in Fig. 1(a). The normalization of $\mathcal{M}_4(\lambda_1, \lambda_2, \lambda_3, \lambda_4)$ is chosen so that the unpolarized Born $gg \rightarrow \gamma\gamma$ cross section reads as

$$\left. \frac{d\sigma_{gg}}{dQ^2 dy dQ_T^2 d\Omega_*} \right|_{Born} = \delta(\vec{Q}_T) \frac{\Sigma_g(\theta_*)}{S} f_{g/h_1}(x_1, \mu_F) f_{g/h_2}(x_2, \mu_F), \quad (10)$$

where

$$\Sigma_g(\theta_*) \equiv \sigma_g^{(0)} L_g(\theta_*), \quad (11)$$

with

$$\sigma_g^{(0)} = \frac{\alpha^2(Q)\alpha_s^2(Q)}{32\pi Q^2(N_c^2 - 1)} \left(\sum_i e_i^2 \right)^2, \quad (12)$$

and

$$L_g(\theta_*) \equiv \sum_{\lambda_1, \lambda_2, \lambda_3, \lambda_4 = \pm 1} |\mathcal{M}_4(\lambda_1, \lambda_2, \lambda_3, \lambda_4)|^2. \quad (13)$$

In these equations, $N_c = 3$ is the number of QCD colors, e_i is the fractional electric charge (in units of the positron charge e) of the quark i circulating in the loop, and $f_{g/h}(x, \mu_F)$ is the gluon PDF evaluated at a factorization scale μ_F . The right-hand side of Eq. (13) includes summation over gluon and photon helicities λ_i , with $i = 1, \dots, 4$.

At NLO, the small- Q_T cross section is proportional to the angular function $\Sigma_g(\theta_*)$ (the same as in the Born cross section), and another function

$$\begin{aligned} \Sigma'_g(\theta_*, \varphi_*) &= \sigma_g^{(0)} \sum_{\lambda_1, \lambda_2, \lambda_3, \lambda_4 = \pm 1} \mathcal{M}_4^*(\lambda_1, \lambda_2, \lambda_3, \lambda_4) \mathcal{M}_4(-\lambda_1, \lambda_2, \lambda_3, \lambda_4) \\ &\equiv \sigma_g^{(0)} L'_g(\theta_*) \cos 2\varphi_*. \end{aligned} \quad (14)$$

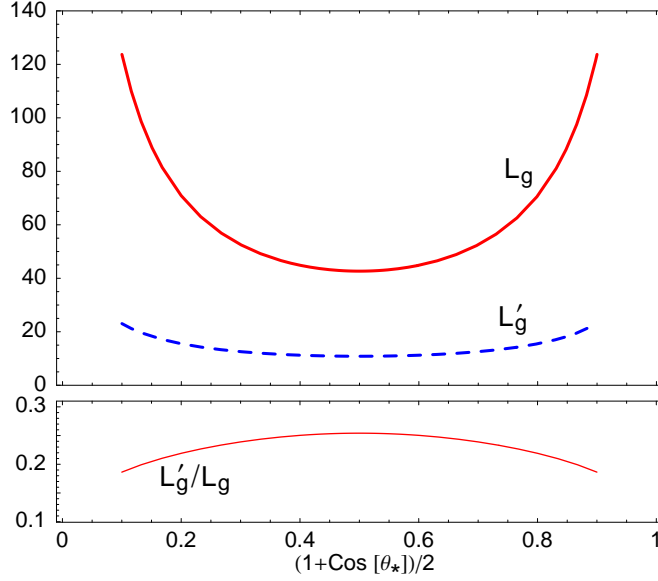


Figure 2: The functions $L_g(\theta_*)$ and $L'_g(\theta_*)$ arising in the $gg \rightarrow \gamma\gamma$ asymptotic cross section (16) and their ratio.

The function $\Sigma'_g(\theta_*, \varphi_*)$ is obtained by spin-averaging the product of the amplitude $\mathcal{M}_4(\lambda_1, \lambda_2, \lambda_3, \lambda_4)$, and the complex-conjugate amplitude $\mathcal{M}_4^*(-\lambda_1, \lambda_2, \lambda_3, \lambda_4)$ evaluated with the reverse sign of the helicity λ_1 . The sign flip for λ_1 results in dependence of $\Sigma'_g(\theta_*, \varphi_*)$ on $\cos 2\varphi_*$. The θ_* dependence of $\Sigma'_g(\theta_*, \varphi_*)$ enters through the function

$$L'_g(\theta_*) = -4\text{Re} \left(M_{1,1,-1,-1}^{(1)} + M_{1,-1,1,-1}^{(1)} + M_{-1,1,1,-1}^{(1)} + 1 \right), \quad (15)$$

presented in terms of reduced amplitudes $M_{\lambda_1, \lambda_2, \lambda_3, \lambda_4}^{(1)}$ in the notation of Ref. [22]. For comparison, the functions $L_g(\theta_*)$ and $L'_g(\theta_*)$ are plotted versus $(1 + \cos \theta_*)/2$ in Fig. 2.

The NLO asymptotic term in the sum of the contributions from the $gg \rightarrow \gamma\gamma$ and $gq_S \rightarrow \gamma\gamma$ channels (denoted as $gg + gq_S$ channel) is

$$A(Q, Q_T, y, \Omega_*) = \frac{1}{S} \left\{ \Sigma_g(\theta_*) \left[\delta(\vec{Q}_T) F_{g,\delta}(Q, y, \theta_*) + F_{g,+}(Q, y, Q_T) \right] + \Sigma'_g(\theta_*, \varphi_*) F'_{g,+}(Q, y, Q_T) \right\}. \quad (16)$$

Here

$$F_{g,\delta} \equiv f_{g/h_1}(x_1, \mu_F) f_{g/h_2}(x_2, \mu_F) \left(1 + 2 \frac{\alpha_s}{\pi} h_g^{(1)}(\theta_*) \right) + \frac{\alpha_s}{\pi} \left\{ \left(\left[\mathcal{C}_{g/a}^{(1,c)} \otimes f_{a/h_1} \right] (x_1, \mu_F) - \left[P_{g/a} \otimes f_{a/h_1} \right] (x_1, \mu_F) \ln \frac{\mu_F}{Q} \right) f_{g/h_2}(x_2, \mu_F) + f_{g/h_1}(x_1, \mu_F) \left(\left[\mathcal{C}_{g/a}^{(1,c)} \otimes f_{a/h_2} \right] (x_2, \mu_F) - \left[P_{g/a} \otimes f_{a/h_2} \right] (x_2, \mu_F) \ln \frac{\mu_F}{Q} \right) \right\}; \quad (17)$$

$$F_{g,+} = \frac{1}{2\pi} \frac{\alpha_s}{\pi} \left\{ f_{g/h_1}(x_1, \mu_F) f_{g/h_2}(x_2, \mu_F) \left(\mathcal{A}_g^{(1,c)} \left[\frac{1}{Q_T^2} \ln \frac{Q^2}{Q_T^2} \right]_+ + \mathcal{B}_g^{(1,c)} \left[\frac{1}{Q_T^2} \right]_+ \right) \right\}$$

$$\begin{aligned}
& + \left[\frac{1}{Q_T^2} \right]_+ \left(\left[P_{g/a} \otimes f_{a/h_1} \right] (x_1, \mu_F) f_{g/h_2}(x_2, \mu_F) \right. \\
& \quad \left. + f_{g/h_1}(x_1, \mu_F) \left[P_{g/a} \otimes f_{a/h_2} \right] (x_2, \mu_F) \right); \tag{18}
\end{aligned}$$

and

$$\begin{aligned}
F'_{g,+} = & \frac{1}{2\pi} \frac{\alpha_s}{\pi} \left[\frac{1}{Q_T^2} \right]_+ \left(\left[P'_{g/g} \otimes f_{g/h_1} \right] (x_1, \mu_F) f_{g/h_2}(x_2, \mu_F) \right. \\
& \left. + f_{g/h_1}(x_1, \mu_F) \left[P'_{g/g} \otimes f_{g/h_2} \right] (x_2, \mu_F) \right). \tag{19}
\end{aligned}$$

The $\mathcal{O}(\alpha_s/\pi)$ coefficients $\mathcal{A}_g^{(1,c)}$, $\mathcal{B}_g^{(1,c)}$ and functions $\mathcal{C}_{g/a}^{(1,c)}(x, b)$, $h_g^{(1)}(\theta_*)$ are defined and listed explicitly in Ref. [6]. The function $h_g^{(1)}(\theta_*)$ denotes an $\mathcal{O}(\alpha_s/\pi)$ correction to the hard-scattering contribution \mathcal{H} in the resummed cross section, cf. Sec. III D. The convolutions $\left[P_{g/a} \otimes f_{a/h} \right]$ and $\left[\mathcal{C}_{g/a}^{(1,c)} \otimes f_{a/h} \right]$, defined for two functions $f(x, \mu_F)$ and $g(x, \mu_F)$ as

$$[f \otimes g](x, \mu_F) \equiv \int_x^1 \frac{d\xi}{\xi} f(\xi, \mu_F) g\left(\frac{x}{\xi}, \mu_F\right),$$

are summed over the intermediate parton's flavors $a = g, q_S$ (gluon and the flavor-singlet combination of quark-scattering channels). In addition to the conventional splitting functions $P_{g/g}(x)$ and $P_{g/q_S}(x)$ arising in $F_{g,+}$, a new splitting function

$$P'_{g/g}(x) = 2C_A(1-x)/x, \tag{20}$$

where $C_A = N_c = 3$, enters the φ_* -dependent part of the asymptotic cross section through $F'_{g,+}$.

For completeness, the small- Q_T asymptotic form Eq. (16) for the $gg + gq_S$ channels is derived in Appendix B. The existence of the φ_* -dependent singular contribution proportional to $\Sigma'_g(\theta_*, \varphi_*)$ is established by examining the factorization of the $2 \rightarrow 3$ cross section in the limit of a collinear gluon emission. It follows directly from factorization rules for helicity amplitudes [8, 9, 10, 11, 12, 13, 14], as well as from the dipole factorization formalism [25].

In contrast, the NLO quark-antiquark contribution $q\bar{q} \rightarrow \gamma\gamma$ does not include a spin-flip contribution, as a result of the simple structure of the Born contribution in $q\bar{q}$ scattering (see also Sec. III C).

B. Resummation

To predict the shape of $d\sigma/dQ_T$ distributions, we perform an all-orders summation of singularities $\delta(\vec{Q}_T)$ and $\left[Q_T^{-2} \ln^p(Q^2/Q_T^2) \right]_+$ in the asymptotic cross section, which coincides with the perturbative expansion of the resummed small- Q_T cross section obtained within the Collins-Soper-Sterman formalism [1, 26, 27]. In this formalism, we write the fully differential cross section as

$$\frac{d\sigma(h_1 h_2 \rightarrow \gamma\gamma)}{dQ dQ_T^2 dy d\Omega_*} = W(Q, Q_T, y, \Omega_*) + Y(Q, Q_T, y, \Omega_*). \tag{21}$$

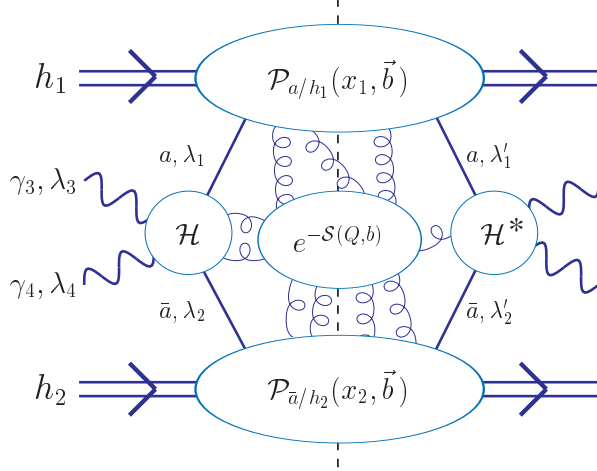


Figure 3: The structure of the resummed form factor $\widetilde{W}(Q, b, y, \Omega_*)$.

The term W contains large logarithmic contributions of the form $\ln^p(Q/Q_T)$ from initial-state radiation, while Y is free of these logs and calculated using collinear QCD factorization (cf. the end of Sec. III D).

The function W may be expressed as a Fourier-Bessel transform of a function $\widetilde{W}(Q, b, y, \Omega_*)$ in the impact parameter (\vec{b}) space,

$$W(Q, Q_T, y, \Omega_*) = \int \frac{d\vec{b}}{(2\pi)^2} e^{i\vec{Q}_T \cdot \vec{b}} \widetilde{W}(Q, b, y, \Omega_*). \quad (22)$$

The generic form of $\widetilde{W}(Q, b, y, \Omega_*)$ in the $q\bar{q} + qq \rightarrow \gamma\gamma$ and $gg + gq_S \rightarrow \gamma\gamma$ channels can be determined by solving evolution equations for the gauge- and renormalization-group invariance of $\widetilde{W}(Q, b, y, \Omega_*)$:

$$\begin{aligned} \widetilde{W}(Q, b, y, \Omega_*) = \sum_a \sum_{\lambda_1, \lambda'_1, \lambda_2, \lambda'_2, \lambda_3, \lambda_4} & \mathcal{H}_a^{\lambda_1 \lambda_2 \lambda_3 \lambda_4}(Q, \Omega_*) \left(\mathcal{H}_a^{\lambda'_1 \lambda'_2 \lambda_3 \lambda_4}(Q, \Omega_*) \right)^* \\ & \times \mathcal{P}_{a/h_1}^{\lambda_1 \lambda'_1}(x_1, \vec{b}) \mathcal{P}_{\bar{a}/h_2}^{\lambda_2 \lambda'_2}(x_2, \vec{b}) e^{-\mathcal{S}_a(Q, b)}. \end{aligned} \quad (23)$$

It is composed of the hard-scattering function $\mathcal{H}_a^{\lambda_1 \lambda_2 \lambda_3 \lambda_4}(Q, \Omega_*)$ and its complex conjugate, $\left(\mathcal{H}_a^{\lambda'_1 \lambda'_2 \lambda_3 \lambda_4}(Q, \Omega_*) \right)^*$; the Sudakov exponential $\exp(-\mathcal{S}_a(Q, b))$; and parton distribution matrices $\mathcal{P}_{a/h_i}^{\lambda_i \lambda'_i}(x_i, \vec{b})$.

The multiplicative structure of Eq. (23) reflects the topology of the dominant cut diagrams in the small- Q_T cross sections shown in Fig. 3. The function $\mathcal{H}_a^{\lambda_1 \lambda_2 \lambda_3 \lambda_4}$ describes the hard $2 \rightarrow 2$ scattering subprocess $a(p_1, \lambda_1) + \bar{a}(p_2, \lambda_2) \rightarrow \gamma(p_3, \lambda_3) + \gamma(p_4, \lambda_4)$, with $a = u, \bar{u}, d, \bar{d}, \dots$ in $q\bar{q} \rightarrow \gamma\gamma$, and $a = \bar{a} = g$ in $gg \rightarrow \gamma\gamma$. All momenta in \mathcal{H} have virtualities of order Q^2 . For now, we consider the leading contribution to $\mathcal{H}_a^{\lambda_1 \lambda_2 \lambda_3 \lambda_4}$, which reads as $\mathcal{H}_a^{\lambda_1 \lambda_2 \lambda_3 \lambda_4} = \sqrt{\sigma_a^{(0)}} \mathcal{M}_4(\lambda_1, \lambda_2, \lambda_3, \lambda_4)$, where the Born helicity amplitude $\mathcal{M}_4(\lambda_1, \lambda_2, \lambda_3, \lambda_4)$ and overall constant normalization $\sigma_a^{(0)}$ are introduced in Sec. III A. Sometimes $\mathcal{H}_a^{\lambda_1 \lambda_2 \lambda_3 \lambda_4}$ also includes finite parts of higher-order $2 \rightarrow 2$ virtual corrections, as discussed in Sec. III D.

Similarly, $\left(\mathcal{H}_a^{\lambda'_1 \lambda'_2 \lambda_3 \lambda_4}(Q, \Omega_*) \right)^*$ arises from the complex-conjugate amplitude $\mathcal{M}_4^*(\lambda_1, \lambda_2, \lambda_3, \lambda_4)$ and possible loop corrections to it. The helicities λ'_1 and λ'_2 in

$(\mathcal{H}_a^{\lambda'_1 \lambda'_2 \lambda_3 \lambda_4})^*$ need not coincide with λ_1 and λ_2 in $\mathcal{H}_a^{\lambda_1 \lambda_2 \lambda_3 \lambda_4}$. The right-hand side of Eq. (23) is summed over flavors a and helicities λ_k, λ'_k of the partons entering $\mathcal{H}\mathcal{H}^*$, as well as over helicities λ_3 and λ_4 of the final-state photons.

The Sudakov exponent

$$\mathcal{S}_a(Q, b) = \int_{C_1^2/b^2}^{C_2 Q^2} \frac{d\bar{\mu}^2}{\bar{\mu}^2} \left[\mathcal{A}_a(C_1, \bar{\mu}) \ln \left(\frac{C_2^2 Q^2}{\bar{\mu}^2} \right) + \mathcal{B}_a(C_1, C_2, \bar{\mu}) \right] \quad (24)$$

resums contributions from the initial-state soft and soft-collinear gluon emission (indicated by gluon lines connecting $e^{-\mathcal{S}}$ to \mathcal{H} , \mathcal{H}^* , and $\mathcal{P}_{a/h}(x, \vec{b})$ in Fig. 3). Here C_1 and C_2 are constants of order unity. The functions $\mathcal{A}_a(C_1, \bar{\mu})$ and $\mathcal{B}_a(C_1, C_2, \bar{\mu})$ can be evaluated in perturbation theory at large scales $\bar{\mu}^2 \gg \Lambda_{QCD}^2$, hence for large Q and small b .

The collinear emissions are described by parton distribution matrices $\mathcal{P}_{a/h}^{\lambda\lambda'}(x, \vec{b})$, where λ and λ' denote the helicity state of the intermediate parton a to the left and right of the unitarity cut in Fig. 3. The matrix $\mathcal{P}_{a/h}^{\lambda\lambda'}(x, \vec{b})$ is derived from a matrix element of the light-cone correlator [28, 29, 30, 31, 32] for finding parton a inside the parent hadron h .

It is convenient to introduce sums of diagonal and off-diagonal entries of the helicity matrix $\mathcal{P}_{a/h}^{\lambda\lambda'}(x, \vec{b})$,

$$\mathcal{P}_{a/h}(x, \vec{b}) = \sum_{\lambda} \mathcal{P}_{a/h}^{\lambda\lambda}(x, \vec{b}), \quad (25)$$

and

$$\mathcal{P}'_{a/h}(x, \vec{b}) = \sum_{\lambda} \mathcal{P}_{a/h}^{\lambda, -\lambda}(x, \vec{b}). \quad (26)$$

In this notation, Eq. (23) can be rewritten as

$$\begin{aligned} \widetilde{W}(Q, b, y, \Omega_*) &= \frac{1}{S} e^{-\mathcal{S}_a(Q, b)} \sum_a \left\{ \Sigma_a(\theta_*) \mathcal{P}_{a/h_1}(x_1, \vec{b}) \mathcal{P}_{\bar{a}/h_2}(x_2, \vec{b}) + \right. \\ &+ \Sigma'_a(\theta_*, \varphi_*) \left[\mathcal{P}'_{a/h_1}(x_1, \vec{b}) \mathcal{P}_{\bar{a}/h_2}(x_2, \vec{b}) + \mathcal{P}_{a/h_1}(x_1, \vec{b}) \mathcal{P}'_{\bar{a}/h_2}(x_2, \vec{b}) \right] \\ &\left. + \Sigma''_a(\theta_*, \varphi_*) \mathcal{P}'_{a/h_1}(x_1, \vec{b}) \mathcal{P}'_{\bar{a}/h_2}(x_2, \vec{b}) \right\}, \quad (27) \end{aligned}$$

where

$$\Sigma_a(\theta_*) \equiv \sum_{\lambda_1, \lambda_2, \lambda_3, \lambda_4} \left| \mathcal{H}_a^{\lambda_1 \lambda_2 \lambda_3 \lambda_4} \right|^2, \quad (28)$$

$$\Sigma'_a(\theta_*, \varphi_*) \equiv \sum_{\lambda_1, \lambda_2, \lambda_3, \lambda_4} \mathcal{H}_a^{\lambda_1 \lambda_2 \lambda_3 \lambda_4} \left(\mathcal{H}_a^{-\lambda_1 \lambda_2 \lambda_3 \lambda_4} \right)^*, \quad (29)$$

and

$$\Sigma''_a(\theta_*, \varphi_*) \equiv \sum_{\lambda_1, \lambda_2, \lambda_3, \lambda_4} \mathcal{H}_a^{\lambda_1 \lambda_2 \lambda_3 \lambda_4} \left(\mathcal{H}_a^{-\lambda_1 - \lambda_2 \lambda_3 \lambda_4} \right)^*. \quad (30)$$

The unpolarized parton distribution $\mathcal{P}_{a/h}(x, \vec{b})$ coincides with the Fourier-Bessel transform of the unpolarized transverse-momentum-dependent (TMD) parton density $\mathcal{P}_{a/h}(x, \vec{k}_T)$ [33] for finding parton a with light-cone momentum fraction x and transverse momentum \vec{k}_T . At small b , $\mathcal{P}_{a/h}(x, \vec{b})$ is reduced to a convolution of unpolarized k_T -integrated parton densities

$f_{a/h}(x, \mu)$ and Wilson coefficient functions $\mathcal{C}_{a/a'}(x, b; C/C_2, \mu)$, evaluated at a factorization scale μ of order $1/b$:

$$\mathcal{P}_{a/h}(x, \vec{b})\Big|_{b^2 \ll \Lambda_{QCD}^{-2}} = \sum_{a'} \left[\int_x^1 \frac{d\xi}{\xi} \mathcal{C}_{a/a'} \left(\frac{x}{\xi}, b; \frac{C_1}{C_2}, \mu \right) f_{a'/h}(\xi, \mu) \right]. \quad (31)$$

Perturbative entries with $\lambda_i = \lambda'_i$ reduce in total to the product of the unpolarized Born scattering probability and unpolarized resummed functions:

$$\begin{aligned} \widetilde{W}(Q, b, y, \Omega_*)\Big|_{\lambda_i = \lambda'_i} &= \sum_a \frac{\Sigma_a(\theta_*)}{S} e^{-S_a(Q, b)} \\ &\times \left[\mathcal{C}_{a/c_1} \otimes f_{c_1/h_1} \right] (x_1, b; \mu) \left[\mathcal{C}_{\bar{a}/c_2} \otimes f_{c_2/h_2} \right] (x_2, b; \mu). \end{aligned} \quad (32)$$

The function $\Sigma_g(\theta_*)$ is shown explicitly in Eq. (11).

C. Spin-flip term in gluon scattering

We concentrate in this subsection on the spin-flip distribution $\mathcal{P}'_{g/h}(x, \vec{b})$ in gluon scattering. Its existence is warranted by basic symmetries of helicity- and transverse-momentum-dependent gluon distribution functions [34]. This function, which describes interference of the amplitudes for nearly collinear gluons with opposite helicities, coincides with the function H^\perp in Ref. [34] up to an overall factor. It contributes to *unpolarized* Q_T distributions, because the hard-scattering product $\mathcal{H}_g^{\lambda_1 \lambda_2 \lambda_3 \lambda_4} \left(\mathcal{H}_g^{\lambda'_1 \lambda'_2 \lambda_3 \lambda_4} \right)^*$ (with $\mathcal{H}_g^{\lambda_1 \lambda_2 \lambda_3 \lambda_4}$ given by the quark box helicity amplitude in Fig. 1(a)) does not vanish for $\lambda_1 = -\lambda'_1$ or $\lambda_2 = -\lambda'_2$. The presence of $\mathcal{P}'_{g/h}(x, \vec{b})$ modifies dependence of the resummed cross section on the photon's azimuthal angle φ_* in the Collins-Soper frame. It vanishes after the integration over φ_* is performed. In contrast, the helicity-diagonal part of $\widetilde{W}(Q, b, y, \Omega_*)$ is independent of φ_* , cf. Eq. (32).

The gluon function $\mathcal{P}'_{g/h}(x, \vec{b})$ is invariant under time reversal (i.e., is T -even) and acquires large contributions proportional to the unpolarized T -even PDF's $\mathcal{P}_{g/h}(x, \vec{b})$ in the process of gluon radiation. These contributions require resummation via PDF evolution equations (similar to Dokshitzer-Gribov-Lipatov-Altarelli-Parisi equations [35, 36, 37, 38]) in order to predict the φ_* dependence in the gg channel.

At one loop, the mixing of spin-flip and unpolarized gluon PDF's is driven by the convolution $\left[P'_{g/g} \otimes f_{g/h} \right] (x, \mu_F)$ of the spin-flip splitting function $P'_{g/g}(x)$ shown in Eq. (20) with the gluon PDF $f_{g/h}(x, \mu_F)$. This convolution may be comparable to or exceed the analogous convolution $\left[P_{g/g} \otimes f_{g/h} \right] (x, \mu_F)$ of the unpolarized splitting function $P_{g/g}(x)$ for some x and μ_F values, as shown in Fig. 4. As a result of the mixing, an additional φ_* -dependent term

$$\begin{aligned} \frac{\Sigma'_g(\theta_*, \varphi_*)}{2\pi S Q_T^2} \frac{\alpha_s}{\pi} &\left(\left[P'_{g/g} \otimes f_{g/h_1} \right] (x_1, \mu_F) f_{g/h_2}(x_2, \mu_F) \right. \\ &\left. + f_{g/h_1}(x_1, \mu_F) \left[P'_{g/g} \otimes f_{g/h_2} \right] (x_2, \mu_F) \right) \end{aligned} \quad (33)$$

arises in the unpolarized $\mathcal{O}(\alpha_s)$ asymptotic piece, cf. Eq. (16). It is produced by the perturbative expansion of the entry proportional to $\Sigma'_g(\theta_*, \varphi_*) \mathcal{P}_{g/h}(x_i, \vec{b}) \mathcal{P}'_{g/h}(x_j, \vec{b})$ in

$\widetilde{W}(Q, b, y, \Omega_*)$, with $\Sigma'_g(\theta_*, \varphi_*)$ shown explicitly in Eqs. (14) and (15). Generally, the φ_* -dependent contribution is not small, even though it is suppressed comparatively to the unpolarized collinear contribution by the ratio $L'_g(\theta_*)/L_g(\theta_*)$ shown in Fig. 2. For example, for $Q = 100$ GeV at the LHC, its magnitude constitutes up to about a half of the collinear unpolarized asymptotic contribution,

$$\frac{\Sigma_g(\theta_*)}{2\pi S Q_T^2} \frac{\alpha_s}{\pi} \left([P_{g/a} \otimes f_{a/h_1}] (x_1, \mu_F) f_{g/h_2}(x_2, \mu_F) + f_{g/h_1}(x_1, \mu_F) [P_{g/a} \otimes f_{a/h_2}] (x_2, \mu_F) \right). \quad (34)$$

The $\mathcal{O}(\alpha_s)$ spin-flip gg contribution does not mix with the gq_S contribution.

In terms of the reduced matrix elements $M_{\lambda_1 \lambda_2 \lambda_3 \lambda_4}^{(1)}$ defined in [22], the double spin-flip hard vertex function $\Sigma''_g(\theta_*, \varphi_*)$ is

$$\Sigma''_g(\theta_*, \varphi_*) = \sigma_g^{(0)} \left(L''_{1g}(\theta_*) + L''_{2g}(\theta_*) \cos(4\varphi_*) \right), \quad (35)$$

where

$$L''_{1g}(\theta_*) = 4\text{Re} \left(M_{1,1,-1,-1}^{(1)} + 1 \right), \quad (36)$$

and

$$L''_{2g}(\theta_*) = 4\text{Re} \left(M_{1,-1,-1,1}^{(1)} M_{1,-1,1,-1}^{(1)*} + 1 \right). \quad (37)$$

The perturbative expansion of the resummed entry proportional to $\Sigma''_g(\theta_*, \varphi_*) P'_{g/h}(x_i, \vec{b}) P'_{g/h}(x_j, \vec{b})$ produces an NNLO term in the unpolarized gg asymptotic piece,

$$\frac{\Sigma''_g(\theta_*, \varphi_*)}{2\pi S Q_T^2} \frac{\alpha_s^2}{\pi^2} \left[P'_{g/g} \otimes f_{g/h_1} \right] (x_1, \mu_F) \left[P'_{g/g} \otimes f_{g/h_2} \right] (x_2, \mu_F). \quad (38)$$

The analogous quark function $\mathcal{P}'_{q_i/h}(x, \vec{k}_T)$ corresponds to the transversity distribution [39] and is odd under time reversal (T -odd). It cannot be generated radiatively through conventional PDF evolution from the T -even unpolarized function $\mathcal{P}_{q_i/h}(x, \vec{k}_T)$ and does not contribute to the NLO asymptotic term. We find $\Sigma'_q = 0$, because the non-vanishing amplitudes $\mathcal{H}_q(q_1^{\lambda_1}, \vec{q}_2^{\lambda_2}, \gamma_3^{\lambda_3}, \gamma_4^{\lambda_4})$ must have opposite helicities of the quark and antiquark ($\lambda_1 = -\lambda_2$). Therefore, the functions $\mathcal{P}'_{q_i/h}(x, \vec{b})$ contribute in pairs through the term proportional to $\Sigma''_q(\varphi_*) = -(\alpha^2 e_i^4 \pi / (2N_c Q^2)) \cos 2\varphi_*$. These contributions are anticipated to be much smaller than the usual spin-average contribution and negligible at large Q , in analogy to unpolarized Drell-Yan production [40, 41].

In summary, the azimuthal angle (φ_*) dependence of photons in the gg scattering channel is affected by large QCD contributions associated with interference between gluons of opposite helicities. These logarithmic corrections may arise at NLO through QCD radiation from conventional unpolarized PDF's, a mechanism that is unique to gluon scattering. Other types of spin-interference contributions (not considered here) involve spin-flip PDF's only. The soft and collinear logarithms associated with the spin-flip contributions must be resummed along the lines discussed in Ref. [42]. Given that $gg \rightarrow \gamma\gamma$ is the subleading production channel at the Tevatron and at the LHC, we henceforth neglect the gluon spin-flip contributions to the resummed $\widetilde{W}(Q, b, y, \Omega_*)$, while subtracting the corresponding φ_* -dependent asymptotic contribution from the finite-order $2 \rightarrow 3$ cross section. The nature of gg spin-flip contributions can be explored by measuring the double-differential distribution in φ_* and Q_T at the LHC, a topic that is interesting also from the point of view of the Higgs boson search. Full resummation of the gluon spin-flip contributions may be needed in the future.

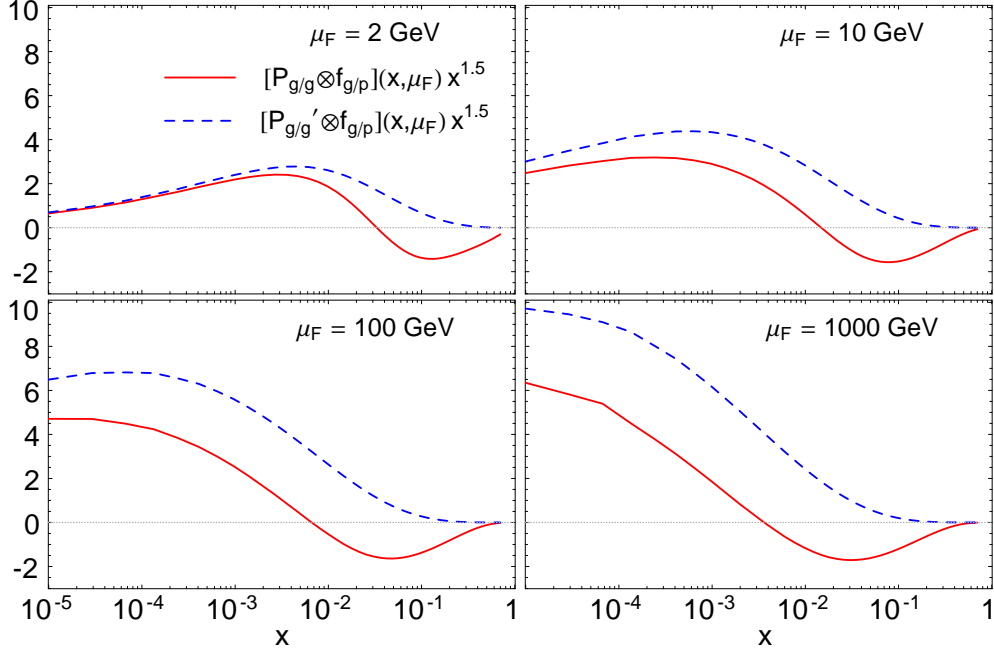


Figure 4: Comparison of $[P_{g/g} \otimes f_{g/p}](x, \mu_F)$ and $[P'_{g/g} \otimes f_{g/p}](x, \mu_F)$ for the gluon PDF $f_{g/p}(x, \mu_F)$ in the proton (multiplied by $x^{1.5}$ to better illustrate the small- x region) at several values of the factorization scale μ_F .

D. Complete expressions for resummed cross sections

In this Section, we review complete expressions for the unpolarized resummed cross sections, starting from the perturbative QCD approximation $\widetilde{W}_{pert}(Q, b, y, \Omega_*)$ valid at small impact parameters $b^2 \ll 1 \text{ GeV}^{-2}$. For a hard-scattering function $\Sigma_{hel.} |\mathcal{H}(Q, \theta_*)|^2 \equiv \Sigma_a(\theta_*) h_a^2(Q, \theta_*)$, the form factor $\widetilde{W}_{pert}(Q, b, y, \Omega_*)$ is

$$\begin{aligned} \widetilde{W}_{pert}(Q, b, y, \theta_*) &= \sum_a \frac{\Sigma_a(\theta_*)}{S} h_a^2(Q, \theta_*) e^{-S_a(Q, b)} \\ &\times \left[\mathcal{C}_{a/c_1} \otimes f_{c_1/h_1} \right] (x_1, b; \mu) \left[\mathcal{C}_{\bar{a}/c_2} \otimes f_{c_2/h_2} \right] (x_2, b; \mu). \end{aligned} \quad (39)$$

The Sudakov function is defined in Eq. (24), and the function $h_a(Q, \theta_*)$ collects radiative contributions to $\mathcal{H}(Q, \theta_*)$ arising at NLO and beyond. We compute the functions h_a , \mathcal{A}_a , \mathcal{B}_a and $\mathcal{C}_{a/c}$ up to orders α_s , α_s^3 , α_s^2 , and α_s , respectively. The \mathcal{A}_a , \mathcal{B}_a and $\mathcal{C}_{a/c}$ coefficients are taken from Refs. [7, 43, 44, 45, 66, 67] and listed in a consistent notation in Ref. [6].

We use a procedure outlined in Ref. [46] to join the small- Q_T resummed cross sections W with the large- Q_T NLO cross sections P . In Eq. (21), $Y \equiv P - A$ is the difference between the perturbative cross section P and its small- Q_T asymptotic expansion A , explicitly given in Eq. (16). For each value of Q and y of the $\gamma\gamma$ pair, $W + Y$ approaches P from above and eventually becomes smaller than P as Q_T increases. We use $W + Y$ as our prediction at Q_T values below this point of crossing and the finite-order cross section P at Q_T above the crossing point.

The final cross sections depend on several factorization scales: C_1/b , C_2Q , $\mu \equiv C_3/b$ in the W term, and $\mu_F \equiv C_4Q$ in the Y term. Here C_i ($i = 1, \dots, 4$) are dimensionless constants

of order unity, chosen as $C_2 = C_4 = 1$, $C_1 = C_3 = 2e^{-\gamma_E} = 1.123\dots$ by default. These choices simplify perturbative coefficients by eliminating scale-dependent logarithmic terms, cf. the appendix in Ref. [6]. Dependence on the scale choice is studied in Section IV.

In the general formulation of CSS resummation presented in [26, 27], one has the freedom to choose different “resummation schemes”, resulting effectively in variations in the form of $h_a(Q, \theta_*)$. These differences are compensated, up to higher-order corrections, by adjustments in the functions \mathcal{B} and \mathcal{C} .

In “the CSS resummation scheme” [1], one chooses $h_a(Q, \theta_*) = 1$, while including the virtual corrections to the $2 \rightarrow 2$ scattering process in \mathcal{B} and \mathcal{C} . In this scheme, some \mathcal{B} and \mathcal{C} coefficients depend on the $2 \rightarrow 2$ hard scattering process and also on θ_* .

In an alternative prescription by Catani, de Florian and Grazzini [47], “the CFG resummation scheme”, one keeps the $2 \rightarrow 2$ virtual corrections within a single function $|\mathcal{H}(Q, \theta_*)|^2$. In this case, the \mathcal{B} and \mathcal{C} functions depend only on the initial state. Most of our numerical calculations are realized in the CSS resummation scheme, with a few made in the CFG scheme for comparison purposes.

In impact parameter (b) space used in the resummation procedure, we must integrate into the nonperturbative region of large b , cf. Eq. (22). Contributions from this region are known to be suppressed at high energies [48], but some residual dependence may remain. In the $q\bar{q} + qq \rightarrow \gamma\gamma$ channel, our model for the nonperturbative contributions (denoted as KN1 [49]) is derived from the analysis of Drell-Yan pair and Z boson production. The nonperturbative function in this model is dominated at large Q by a soft contribution, which does not depend on the flavor of initial-state light quarks. This function is therefore expected to be applicable to the $q\bar{q} + qq \rightarrow \gamma\gamma$ process.

The nonperturbative function in the $gg + gg_S$ channel, which is yet to be measured directly, is approximated by the nonperturbative function for the $q\bar{q} + qq$ channel multiplied by the ratio $C_A/C_F = 9/4$ of the color factors C_A and C_F for the leading soft contributions in the gg and $q\bar{q}$ channels. This ansatz suggests stronger dependence of the $gg + gg_S$ channel on the nonperturbative input compared to the $q\bar{q} + qq$ channels. It leads to small differences from the prescription used in Refs. [7, 20], where only the leading $\ln Q$ term of the nonperturbative function was rescaled. To examine the dependence of the resummed cross sections on the nonperturbative model, we evaluate some of them assuming an alternative (BLNY) parameterization of the nonperturbative function [50].

IV. NUMERICAL RESULTS

The analytical results of Sec. III are implemented in our computer codes LEGACY and RESBOS [46, 50, 51, 52]. We use the same parameters as in the calculation of Ref. [5], and we concentrate on the region $Q_T < Q$ where our calculation is most reliable [5].

A. Results for Run 2 at the Tevatron

In this section, we present our results for the Tevatron $p\bar{p}$ collider at $\sqrt{S} = 1.96$ TeV. We make the same restrictions on the final-state photons as those used in the experimental measurement by the Collider Detector at Fermilab (CDF) collaboration [53]: transverse momentum $p_T^\gamma > p_{T\min}^\gamma = 14$ (13) GeV for the harder (softer) photon, and rapidity $|y^\gamma| < 0.9$ for each photon. We impose photon isolation by requiring the hadronic transverse energy

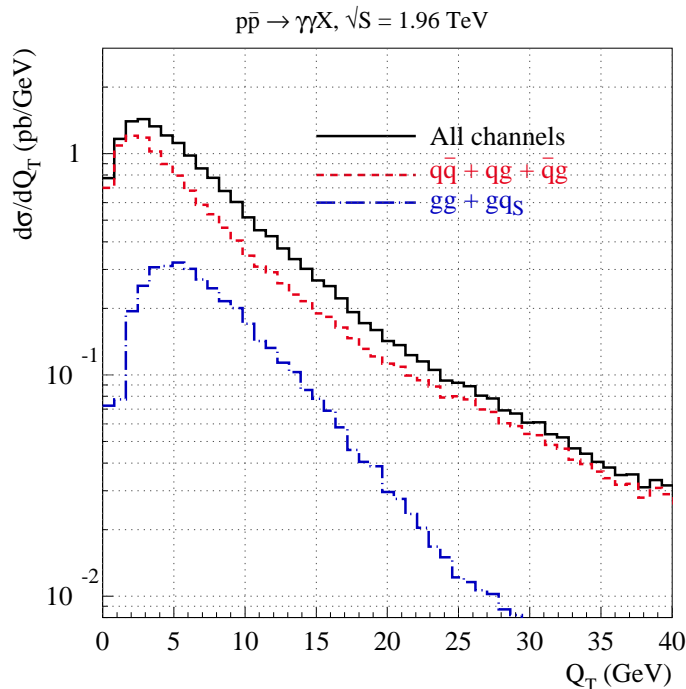


Figure 5: Parton flavor decomposition of the resummed transverse momentum distribution at the energy $\sqrt{S} = 1.96 \text{ TeV}$ of the Tevatron Run-2. The total (solid), $q\bar{q} + qg$ (dashes), and $gg + gq_S$ (dash-dots) initial-state contributions are shown separately.

not to exceed 1 GeV in the cone $\Delta R = 0.4$ around each photon, as specified in the CDF publication. We also require the angular separation $\Delta R_{\gamma\gamma}$ between the photons to be larger than 0.3.

We focus in this paper on the role of the gg contribution, referring to our other papers [5, 6] for a more complete treatment.

To illustrate the relative importance of the individual initial-state contributions in the final answer, we provide a parton flavor decomposition of our resummed transverse momentum distribution $d\sigma/dQ_T$ in Fig. 5. This distribution is integrated over all diphoton invariant masses Q , subject to the CDF cuts, and receives dominant contributions from the $Q_T < Q$ region. The $gg + gq_S$ contribution supplies about one-third of the total rate near $Q_T = 5 \text{ GeV}$. It falls steeply after $Q_T > 20 \text{ GeV}$, because the gluon PDF falls steeply with parton fractional momentum x .

Dependence of the resummed cross sections on the choice of factorization scales mentioned in Section IIID is examined in Fig. 6. We pick a few characteristic combinations of alternative scales to probe the scale dependence associated with the resummed Sudakov function e^{-S} , the b -dependent PDF's $\mathcal{P}_{a/h}(x, \vec{b}) \approx [C_{a/c} \otimes f_{c/h}](x, b; \mu)$, and the regular Y term. The small- Q_T region is sensitive primarily to the scales $C_1/b, C_2 Q, C_3/b$ in the resummed term W . The event rate at large Q_T is controlled by the choice of the factorization scale $\mu_F \equiv C_4 Q$ in the regular term Y .

At the relatively low values of Q relevant for the Tevatron experiments, the scale dependence of the next-to-leading order $gg + gq_S$ cross section is still substantial, with variations being about -20% ($+50\%$) at $Q_T = 5 - 10 \text{ GeV}$, $\pm 10\%$ at $Q_T = 10 - 20 \text{ GeV}$, and $\pm 20\%$

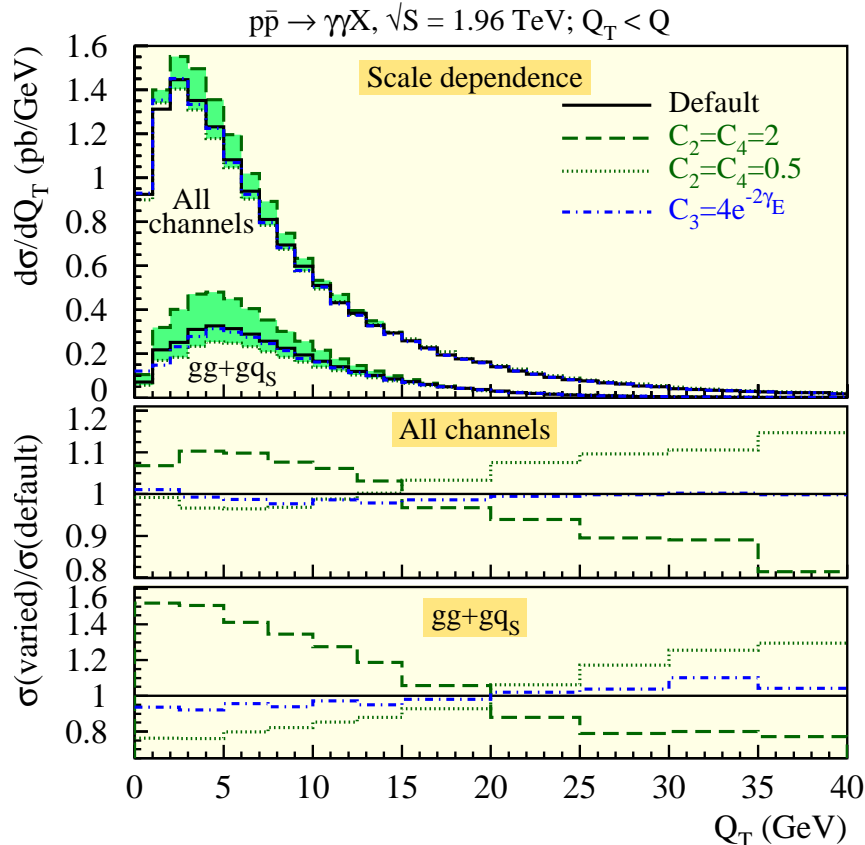


Figure 6: Scale dependence of the cross sections in $gg + gq_S$ and all scattering channels. The upper frame shows cross sections for the default choice of scales specified in Section III D (solid), as well as for varied scales $C_2 = C_4 = 2$ (dashes), $C_2 = C_4 = 0.5$ (dots), and $C_3 = 4e^{-2\gamma_E}$ (dot-dashes). The lower two frames show ratios of the cross sections computed for the varied factorization scales to the cross section for the default choice of the scales.

at $Q_T = 20 - 40$ GeV. Since the Y term is the lowest-order approximation for $gg \rightarrow \gamma\gamma g$ at $Q_T \sim Q$, the scale dependence associated with the constant C_4 remains pronounced at large Q_T . The inclusive $gg + gq_S$ rate, integrated over Q_T , varies by 20 – 40% almost independently of the $\gamma\gamma$ invariant mass Q . The large scale dependence of the NLO $gg + gq_S$ cross section reflects slow perturbative convergence in gluon gluon scattering, observed also in other similar processes, e.g., $gg \rightarrow$ Higgs via the top quark loop [54, 55, 56]. For this reason, a NNLO calculation would be desirable to reduce the scale uncertainty in the $gg + gq_S$ channel.

On the other hand, the scale dependence of the cross section when all channels are combined is relatively mild, with variations not exceeding 10% at small Q_T and 20% at large Q_T . Variations in the integrated inclusive rate for all channels combined are below 10% at $Q > 30$ GeV.

Another aspect of scale dependence is associated with the assumed arrangement of logarithmic terms in the resummed W term, i.e., the “resummation scheme” that is adopted. This dependence is yet another indicator of the size of higher-order corrections not included in the present analysis. Figure 7(a) shows ratios of the full resummed cross sections in the Catani-de Florian-Grazzini (CFG) and Collins-Soper-Sterman (CSS) resummation schemes,

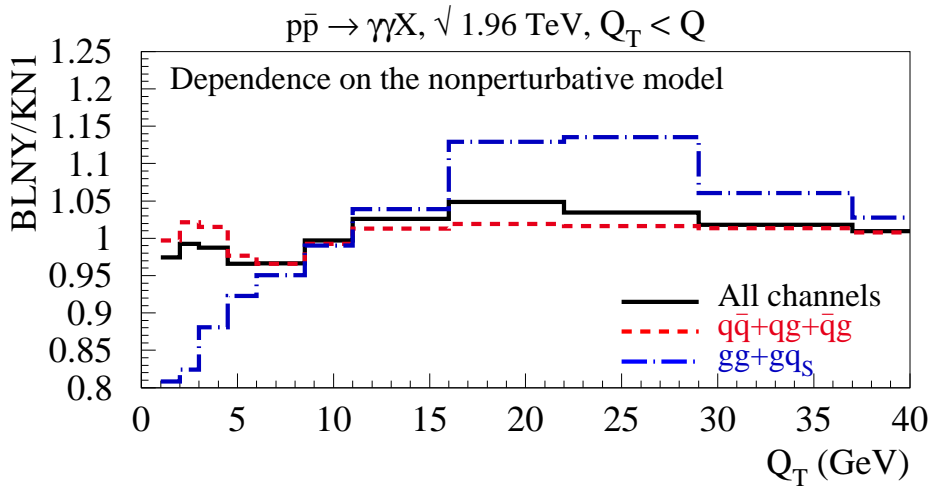
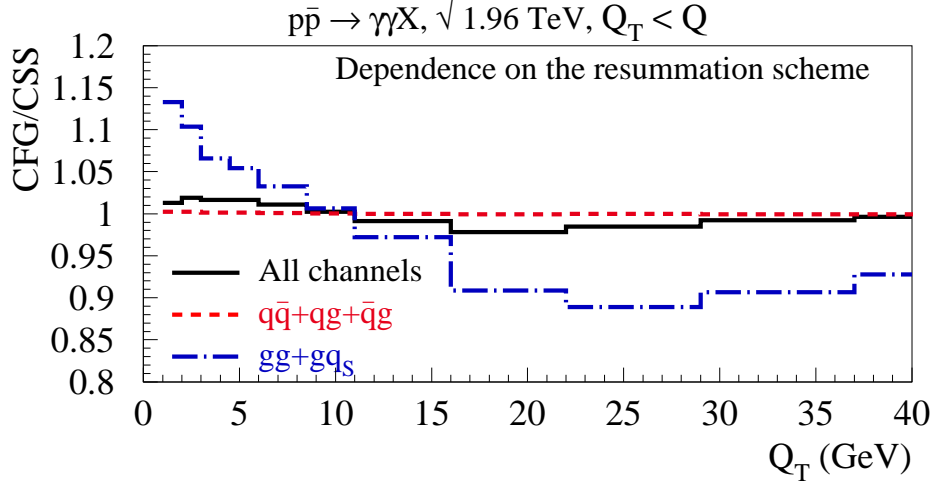


Figure 7: Ratios of resummed cross sections at the Tevatron Run-2 computed in (a) the Catani-de Florian-Grazzini (CFG) and Collins-Soper-Sterman (CSS) resummation schemes and (b) using the BLNY and KN1 nonperturbative models, as functions of the $\gamma\gamma$ transverse momentum Q_T . The ratios are shown in the $q\bar{q} + qg$ (dashed), $gg + gq_S$ (dot-dashed), and all (solid) scattering channels. A $Q_T < Q$ cut is imposed in this comparison.

as described in Sec. III. The differences between these schemes stem from the different treatment of the NLO hard-vertex correction $h_a^{(1)}(\theta_*)$. The magnitude of $h_a^{(1)}(\theta_*)$ determines whether the channel is sensitive to the choice of the two resummation schemes. The magnitude of $h_g^{(1)}(\theta_*)$ in the $gg + gq_S$ channel exceeds that of $h_q^{(1)}(\theta_*)$ in the $q\bar{q} + qg$ channel by roughly an order of magnitude for most values of the θ_* angle [43]. Consequently, while the dependence on the resummation scheme is practically negligible in the dominant $q\bar{q} + qg$ channel (dashed line), it can reach 15% in the subleading $gg + gq_S$ channel (dot-dashed line). The Q_T spectrum in $gg + gq_S$ channel is slightly softer in the CFG scheme up to the point of switching to the fixed-order cross section at $Q_T \approx 60$ GeV. The resummation scheme dependence in all channels (solid line) is less than 3-4%, reflecting mostly the scheme dependence in the $gg + gq_S$ channel.

To examine the sensitivity of the resummed predictions to long-distance nonperturbative dynamics in hadron-hadron scattering, we include in Fig. 7(b) a comparison with the resummed cross sections for an alternative choice of the nonperturbative model. As explained in Sec. IIID, our default calculation is performed in the recent KN1 model [49] for the nonperturbative part of the resummed form factor $\widetilde{W}(Q, b, y, \Omega_*)$. Figure 7(b) shows ratios of the predictions for a different BLNY model [50] and our default KN1 model in various initial-state scattering channels.

The difference is maximal at the lowest Q_T , as expected, and it is less than 5% for the total cross section. For the $q\bar{q} + gg$ and $gg + gg_S$ initial states the maximal difference is about 5% and 20%, respectively. The dependence on the nonperturbative function is stronger in the $gg + gg_S$ channel, where the BLNY/KN1 ratio in the $gg + gg_S$ channel reaches its maximum of 1.15 at $Q_T \approx 25$ GeV and slowly decreases toward 1, reached at the switching point at $Q_T \approx 60$ GeV. This behavior reflects our assumption of a larger magnitude of the nonperturbative function in the $gg + gg_S$ channel, which is rescaled in our model by $C_A/C_F = 9/4$ compared to the nonperturbative function in the $q\bar{q} + gg$ channel. In summary, despite a few-percent uncertainty associated with the nonperturbative function in the $gg + gg_S$ process, the overall dependence of the Tevatron $\gamma\gamma$ cross section on the nonperturbative input can be neglected.

B. Results for the LHC

To obtain predictions for pp collisions at the LHC at $\sqrt{S} = 14$ TeV, we employ the cuts on the individual photons used by the ATLAS collaboration in their simulations of Higgs boson decay, $h \rightarrow \gamma\gamma$ [2]. We require transverse momentum $p_T^\gamma > 40$ (25) GeV for the harder (softer) photon, and rapidity $|y^\gamma| < 2.5$ for each photon. We impose the ATLAS isolation criteria, looser than for the Tevatron study, requiring less than 15 GeV of hadronic and extra electromagnetic transverse energy inside a $\Delta R = 0.4$ cone around each photon. We also require the separation $\Delta R_{\gamma\gamma}$ between the two isolated photons to be above 0.4. The cuts optimized for the Higgs boson search may require adjustments in order to test perturbative QCD predictions in the full $\gamma\gamma$ invariant mass range accessible at the LHC.

Distributions in the invariant mass Q , transverse momentum Q_T , and azimuthal angle separation $\Delta\varphi \equiv \varphi_{\gamma_1} - \varphi_{\gamma_2}$ between the two photons in the laboratory frame are shown in Fig. 8. As before, we compare the magnitudes of the $q\bar{q} + gg$ and $gg + gg_S$ cross sections. The qualitative features are similar to those at the Tevatron, but the relative contribution of the various initial states changes at the LHC. The $gg + gg_S$ initial state contributes about 25% of the total rate at $Q \sim 80$ GeV where the mass distribution peaks, but the $gg + gg_S$ rate falls faster than $q\bar{q} + gg$ with increasing invariant mass.

In the invariant mass range relevant for the Higgs boson search, $115 < Q < 140$ GeV, the transverse momentum distribution in Fig. 8(b) shows that the $gg + gg_S$ initial state accounts for about 25% of the rate at low Q_T . At high transverse momentum, on the other hand, the other channels dominate. The relative size of the $gg + gg_S$ contribution drops as the invariant mass or the transverse momentum of the photon pair grows. The $gg + gg_S$ contribution falls more steeply with Q_T for larger masses of the diphoton. These features are attributable to the steeply falling gluon distribution as a function of increasing momentum fraction x .

The scale dependence at the LHC, presented in Fig. 9, is somewhat reduced compared to the Tevatron (cf. Fig. 6). Maximum scale variations of about 40% in the $gg + gg_S$ channel are observed at the peak of the $d\sigma/dQ_T$ distribution, and they are substantially smaller at

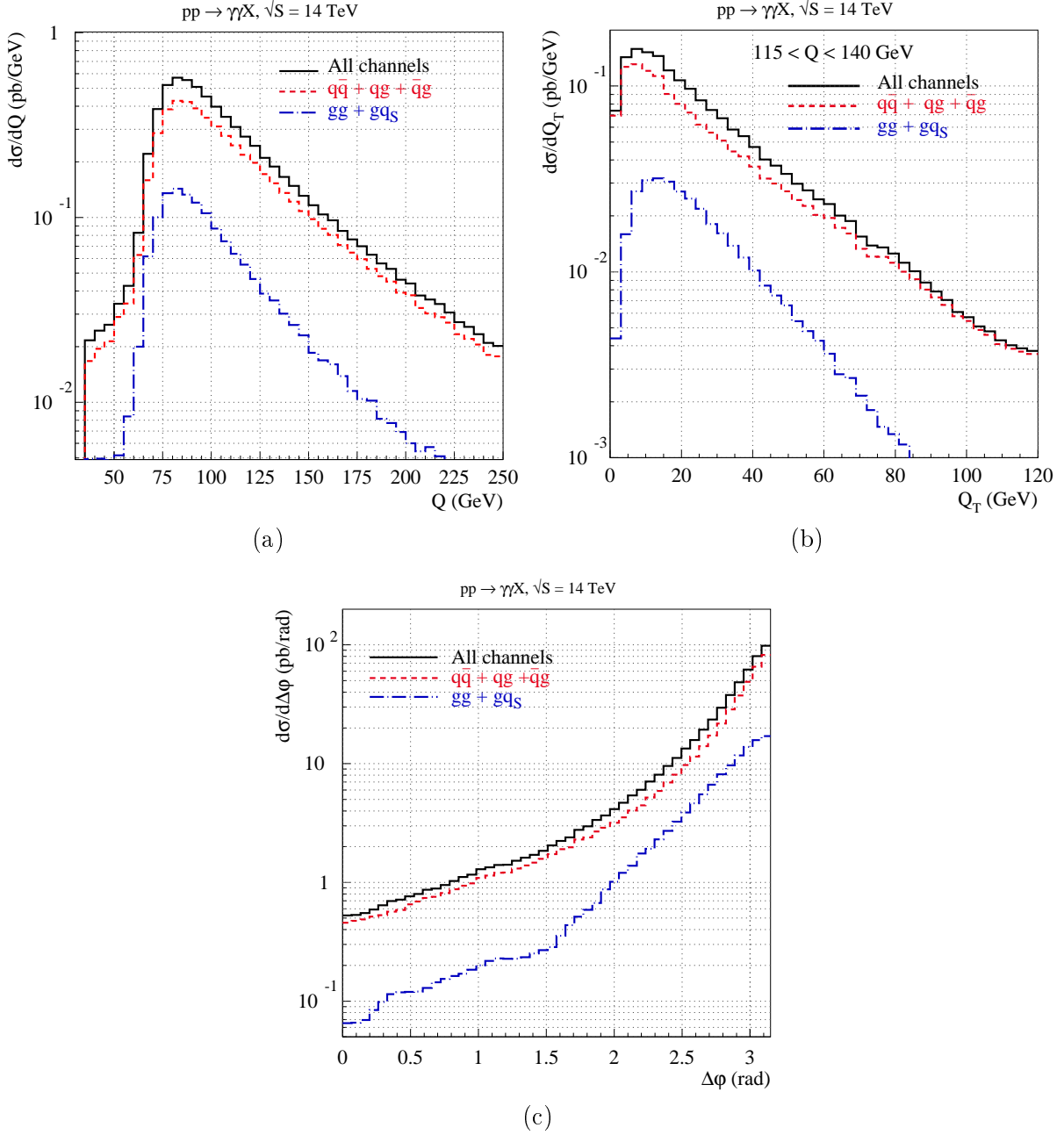


Figure 8: Resummed $d\sigma/dQ$, $d\sigma/dQ_T$, and $d\sigma/d\Delta\phi$ distributions of photon pairs at the LHC for ATLAS kinematic cuts.

large Q_T . The scale variation in the sum over all channels does not exceed 10% (15%) at small Q_T (large Q_T). Variations in the integrated inclusive rate at $Q > 50$ GeV are below 7% (30%) in all channels ($gg + gq_S$ channel).

The dependence on the resummation scheme is mild at the LHC (cf. Fig. 10(a)), with the maximal differences between the CSS and CFG schemes below 0.5%, 10%, and 2% in $q\bar{q} + qg$, $gg + gq_S$, and all channels. The scheme dependence is again the largest in the $gg + gq_S$ channel, where it persists up to the point of switching to the fixed-order cross section at $Q_T \approx 120$ GeV. The ratios of the resummed cross sections calculated in the BLNY and KN1

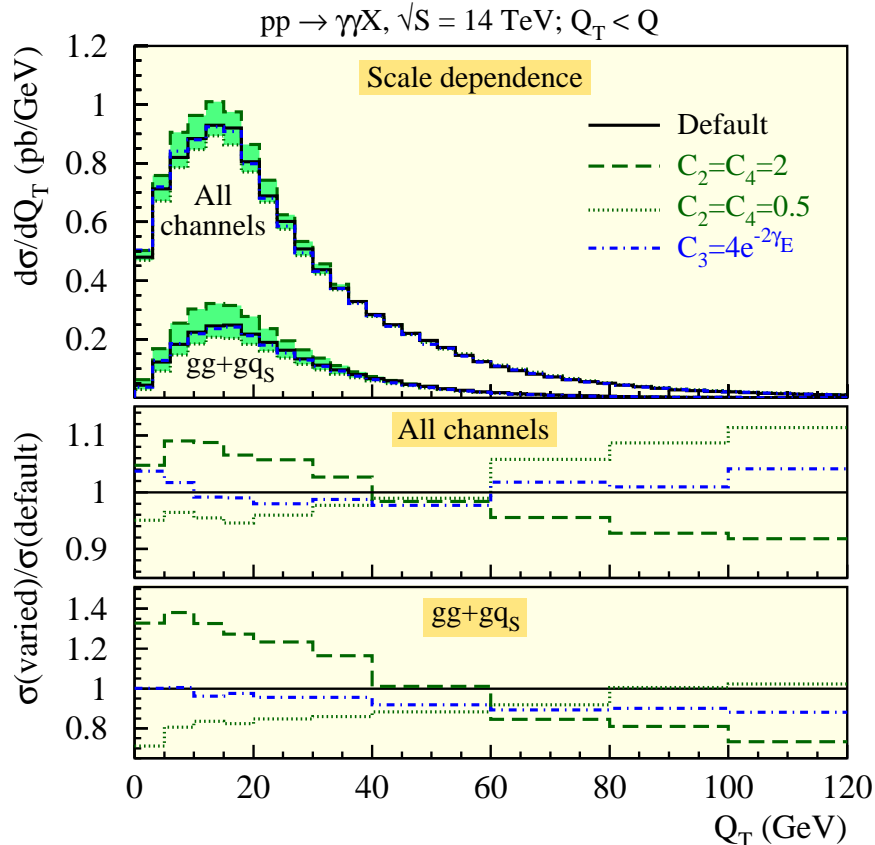


Figure 9: Scale dependence in the $gg + gq_S$ and all scattering channels at the LHC for the same scale choices as in Fig. 6.

models for nonperturbative contributions in the CSS scheme are shown in Fig. 10(b). The influence of the long-distance (large- b) contributions is suppressed at the high center-of-mass energy of the LHC. Differences between the predictions in the two models do not exceed 2%, 6%, and 2% in the $q\bar{q} + qg$, $gg + gq_S$, and all scattering channels.

The KN1 and BLNY nonperturbative models neglect the possibility of a strong x dependence of the nonperturbative function, which may substantially modify our predictions at the energy of the LHC collider. Analysis of small- x semi-inclusive deep inelastic scattering data [57] suggests that x -dependent nonperturbative corrections of uncertain magnitude may substantially affect the resummed cross sections. Such corrections can be constrained by studying the rapidity and energy dependence of the nonperturbative function at the Tevatron and LHC, for example, from copious production of Z bosons [57]. We conclude that uncertainties due to the choice of the resummation scheme and the nonperturbative model will be small at the LHC, if the resummed nonperturbative function does not vary strongly with x .

C. The role of the gq_S contribution

Figures 5-10 show the contributions from the $q\bar{q} + qg$ and $gg + gq_S$ channels along with their sum. One may wonder if a further decomposition into $q\bar{q}$ and qg (or gg and gq_S) contri-

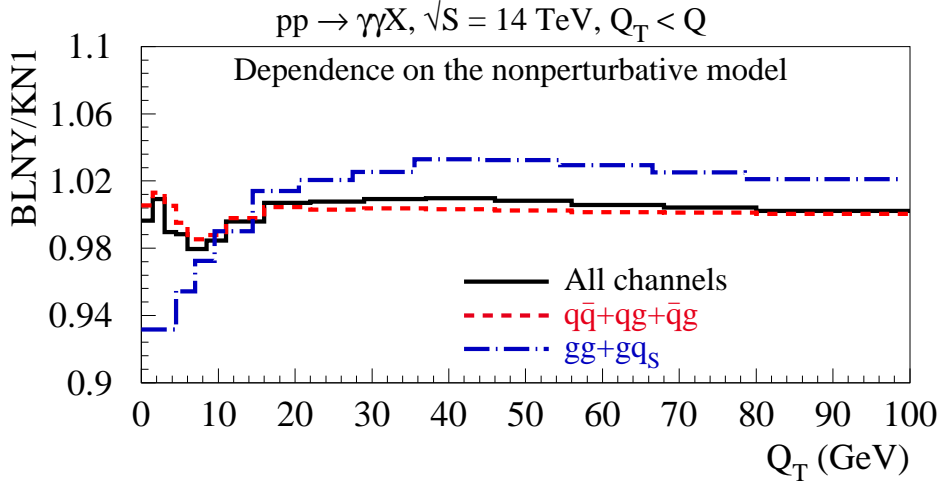
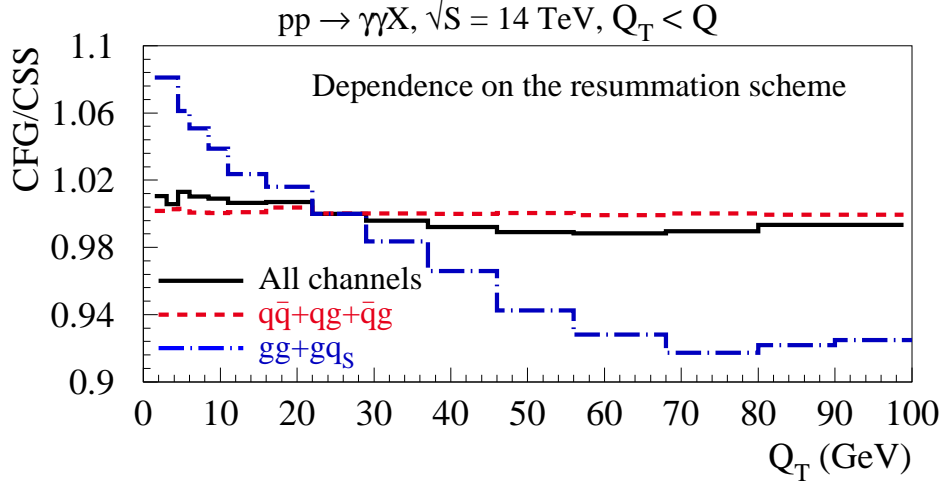


Figure 10: Same as Fig. 7, at the LHC.

butions could provide additional insights into the relative importance of different scattering processes. We observe in our calculations that the resummed cross sections $W + Y$ and the fixed-order cross sections P in the elementary scattering subchannels ($q\bar{q}, qg, \dots$) may not cross until Q_T is significantly larger than Q . This result is at variance with our expectation that the fixed-order answer should be adequate when Q_T is of order Q , where logarithmic effects are small, and the one-scale nature of the dynamics seems apparent.

Consider, for example, the gg and $gg + gq_s$ transverse momentum distributions in the mass interval $115 < Q < 140$ GeV at the LHC shown in Figs. 11(a) and (b). In the gg channel alone (Fig. 11(a)), the $W + Y$ cross section remains above the NLO cross section P until $Q_T \sim 140$ GeV. However, after the gq_s contribution is included (Fig. 11(b)), $W + Y$ crosses P at $Q_T \sim 105$ GeV. Our expectation of the adequacy of the NLO prediction at $Q_T \sim Q$ is satisfied in this case, and this conclusion also holds for other intervals of Q . At the crossing point, the two cross sections satisfy $W + Y = P$, i.e., $W = A$; the resummed term is equal to its NLO perturbative expansion, the asymptotic term. Similarly, good matching of the resummed and NLO cross sections in the $q\bar{q} + qg$ channel requires that we include

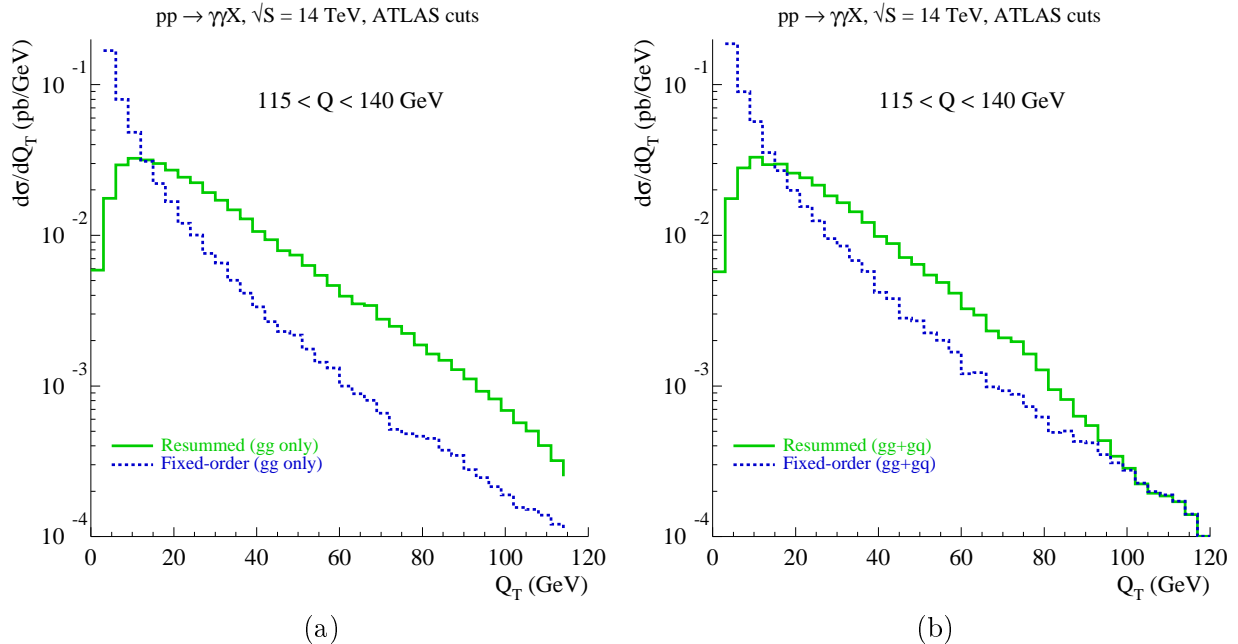


Figure 11: Inclusion of the qg contribution improves the matching of the resummed and NLO perturbative cross sections at large Q_T , as demonstrated by these plots of the resummed and finite-order NLO cross sections for (a) the gg channel only; (b) the combined $gg + gg_S$ channel. The resummed and NLO cross sections are shown by the solid and dashed lines.

both $q\bar{q}$ and qg contributions.

This feature can be understood by noticing that the flavors of the PDF's $f_{a/h}(x, \mu)$ mix in the process of PDF evolution. Consequently the perturbative expansion of W in the gg channel contains the full NLO asymptotic piece A in the combined $gg + gg_S$ channel, generated from the Sudakov exponential and lowest-order resummed contribution $\propto f_{g/h_1}(x_1, 1/b) f_{g/h_2}(x_2, 1/b)$ evaluated at a scale of order $1/b$. The mismatch between the flavor content in the perturbatively expanded W and A in nominally the same gg subchannel causes the difference $W - A$ to be large and delays the crossing. On the other hand, the flavor content of W and A is the same (up to NNLO) when the gg and gg_S contributions are combined, and the matching is improved. The gg_S scattering subchannel has been assumed to be small and neglected in past studies, and indeed it contributes about one tenth of the $gg + gg_S$ inclusive rate $d\sigma/dQ$. However, we see that the gg_S contribution must be included to correctly predict $d\sigma/dQ_T$ and to realize matching between the resummed and perturbative contributions at large transverse momenta.

V. SUMMARY AND CONCLUSIONS

In this paper, we address new theoretical issues in Q_T resummation at two-loop accuracy that arise in the gluon-gluon subprocess, $gg + gq \rightarrow \gamma\gamma$, one of the important short-distance subprocesses that contribute to the inclusive reactions $p\bar{p} \rightarrow \gamma\gamma X$ at the Fermilab Tevatron and $pp \rightarrow \gamma\gamma X$ at the CERN Large Hadron Collider (LHC).

We evaluate all next-to-leading (NLO) contributions of order $\mathcal{O}(\alpha^2\alpha_s^3)$ to the $gg+gq \rightarrow \gamma\gamma$

process (Fig. 1(b-e)). A new ingredient in this paper is the inclusion of the $gq \rightarrow \gamma\gamma q$ process, Fig. 1(d), a necessary component of the resummed NLO contribution. We resum to next-to-next-to-leading logarithmic (NNLL) accuracy the large logarithmic terms of the form $\ln(Q_T^2/Q^2)$ in the limit when Q_T of the $\gamma\gamma$ pair is smaller than its invariant mass Q . The perturbative Sudakov functions \mathcal{A} and \mathcal{B} and the Wilson coefficient functions \mathcal{C} in the resummed cross section W are computed to orders α_s^3 , α_s^2 , and α_s . The resummed cross sections are computed according to the CSS [1] and CFG [47] resummation schemes, with the differences between the two approaches reflecting the size of higher-order corrections. A new nonperturbative function [49], dominated by a process-independent soft correction, is employed to describe the dynamics at large impact parameters.

Subtraction of the singular logarithmic contributions associated with initial-state radiation from the NLO cross section P defines a regular piece Y . This regular term is added to the small- Q_T resummed cross section W to predict the production rate at small to moderate values of Q_T . In the gg channel, we also subtract from P a new singular spin-flip contribution that affects azimuthal angle (φ_*) dependence in the Collins-Soper reference frame. For our final prediction, we switch from the resummed cross section $W + Y$ to P at the point where $W + Y$ crosses P , approaching P from above, as in Ref. [46]. The location of this point in Q_T is of order Q in the $q\bar{q} + qg$ and the $gg + gq$ channels. For such matching to happen, it is essential to combine cross sections in the $q\bar{q}$ and qg (gg and gq) channels, as demonstrated in Sec. IV C.

At the LHC (Tevatron), the $gg + gq$ subprocess contributes 20% (10%) of the total $\gamma\gamma$ production rate (integrated over the full range of the photons' momenta). The relative contribution of $gg + gq$ scattering may reach 25% for some Q and Q_T values. The $gg + gq$ channel provides an interesting opportunity to test CSS resummation at a loop level and may be explored in detail at later stages of the LHC operation. The NNLL/NLO resummed cross section for the $gg + gq_S$ channel is used in Ref. [6] to predict fully differential distributions of Higgs bosons and QCD background at the LHC in the Higgs $\rightarrow \gamma\gamma$ decay mode.

Acknowledgments

Research in the High Energy Physics Division at Argonne is supported in part by US Department of Energy, Division of High Energy Physics, Contract DE-AC02-06CH11357. The work of C.-P. Y. is supported by the U. S. National Science Foundation under grant PHY-0555545. P.M.N. thanks G. Bodwin for discussions of the azimuthal angle dependence in gluon scattering. We gratefully acknowledge the use of *Jazz*, a 350-node computing cluster operated by the Mathematics and Computer Science Division at ANL as part of its Laboratory Computing Resource Center. The Feynman diagrams in Fig. 1 were drawn with aid of the program JAXODRAW [58].

Appendix A: THE $gq_S \rightarrow \gamma\gamma q_S$ AMPLITUDE

To obtain the gluon-quark contribution to the $gg + gq_S$ scattering channel shown in Fig. 1(d), we derive the helicity-dependent $q\bar{q}\gamma\gamma g \rightarrow 0$ amplitude $\mathcal{M}_5(q_1, \bar{q}_2, \gamma_3, \gamma_4, g_5)$ from the one-loop $q\bar{q}ggg$ amplitude in the color-decomposed representation available in Ref. [8].

The $q\bar{q}\gamma\gamma g$ amplitude is expressed as

$$\mathcal{M}_5(q_1^{c_1}, \bar{q}_2^{c_2}, \gamma_3, \gamma_4, g_5^{a_5}) = 2g^3 e^2 \left(\sum_{i_i} e_{i_i}^2 \right) T_{c_1 c_2}^{a_5} \sum_{\sigma \in S_3^{(345)}} A_{5;1}^{L,[1/2]}(1_q, 2_{\bar{q}}; \sigma(3), \sigma(4), \sigma(5)) \quad (\text{A1})$$

in terms of the primitive amplitudes $A_{5;1}^{L,[1/2]}(1_q, 2_{\bar{q}}; 3, 4, 5) = -A_{5;1}^f(1_q, 2_{\bar{q}}; 3, 4, 5) - A_{5;1}^s(1_q, 2_{\bar{q}}; 3, 4, 5)$ for $q\bar{q}ggg \rightarrow 0$ scattering involving a spin-1/2 fermion loop. The amplitude \mathcal{M}_5 is proportional to the sum $\sum_{i_i} (e^2 e_{i_i}^2)$ of squared quark charges circulating in the fermion loop, as well as the QCD generator matrix $T_{c_1 c_2}^{a_5}$, with $\text{Tr}(T^{a_1} T^{a_2}) = \delta^{a_1 a_2}$. The color indices c_1 , c_2 , and a_5 belong to the quark 1, antiquark 2, and gluon 5. The primitive amplitudes are summed over all possible permutations $S_3^{(345)}$ of the legs 3, 4, and 5.

Equation (A1) is derived from Eq. (2.10) of Ref. [8] after gluons 3 and 4 are replaced with photons, i.e., the QCD generators T^{a_3} and T^{a_4} are replaced by identity matrices, and the overall charge factor is adjusted, $g^5 \rightarrow 2g^3 \sum_{i_i} (e e_{i_i})^2$. It correctly reproduces the small- Q_T asymptotic behavior reflected in Eq. (16), which we derive by applying factorization relations in the splitting amplitude formalism discussed in Appendix B. The $q\bar{q}\gamma\gamma g$ amplitude in Eq. (A1) disagrees with the one published in Ref. [24] which appears to violate factorization relations in the $q \parallel \bar{q}$ limit. A few independent amplitudes $A_{5;1}^f(1_q, 2_{\bar{q}}; 3, 4, 5)$ and $A_{5;1}^s(1_q, 2_{\bar{q}}; 3, 4, 5)$ are presented explicitly in Sec. 5 of Ref. [8], with the remaining amplitudes related by discrete symmetries according to Eq. (5.25) in that publication. Some $q\bar{q}ggg$ amplitudes contain infrared poles, which cancel in the sum over permutations $S_3^{(345)}$. We retain only non-vanishing finite parts F^x of such divergent amplitudes, i.e., we take $A_{5;1}^x = iF^x/(16\pi^2)$ for $x = f$ and s .

Appendix B: DERIVATION OF THE SMALL- Q_T ASYMPTOTIC TERM FOR GLUON-GLUON SCATTERING

In this appendix, we derive the small- Q_T asymptotic approximation Eq. (16) for the NLO cross section in $g_1 g_2 \rightarrow \gamma_3 \gamma_4$ scattering. We expand the finite-order cross section as a series in the small parameter Q_T^2/Q^2 . Consider first the leading real-emission contributions, which arise when gluon 5 is radiated off the external gluon leg 1 or 2 as in Fig. 1(b).¹ In the notation introduced in Sec. III, the small- Q_T approximation for the real-emission cross section takes the form

$$A(Q, Q_T, y, \Omega_*)|_{real} = \int_{x_1}^1 d\xi_1 \int_{x_2}^1 d\xi_2 f_{g/h_1}(\xi_1, \mu_F) f_{g/h_2}(\xi_2, \mu_F) \frac{1}{(2\pi)^4} \frac{1}{64\xi_1 \xi_2 S} |\mathcal{M}_5|^2 \times \left\{ \frac{\delta(\xi_1 - x_1)}{[1 - \hat{x}_2]_+} + \frac{\delta(\xi_2 - x_2)}{[1 - \hat{x}_1]_+} - x_1 x_2 \delta(\xi_1 - x_1) \delta(\xi_2 - x_2) \ln \frac{Q_T^2}{Q^2} \right\}. \quad (\text{B1})$$

The right-hand side of Eq. (B1) includes a product of the gluon parton densities $f_{g/h_i}(\xi_{1,2}, \mu_F)$, squares of parton-scattering amplitudes \mathcal{M}_5 , and phase-space factors, integrated over the light-cone momentum fractions $\xi_{1,2} \equiv p_{1,2}^+/P_{1,2}^+$ of the incoming gluons 1

¹ In contrast, Feynman graphs with gluon radiation off a propagator in the quark loop [Fig. 1(c)] are finite in the $Q_T \rightarrow 0$ limit.

and 2. The delta-functions constrain integration to phase-space regions where the final-state gluon 5 is collinear to gluon 1 [$p_5^\mu = (1 - \hat{x}_1)p_1^\mu$], collinear to gluon 2 [$p_5^\mu = (1 - \hat{x}_2)p_2^\mu$], or soft [$p_5^\mu \rightarrow 0$], with $\hat{x}_i \equiv x_i/\xi_i$ for $i = 1, 2$.

The $2 \rightarrow 3$ helicity amplitude $\mathcal{M}_5(1, 2, 3, 4, 5)$ is analyzed conveniently in an unphysical scattering channel $0 \rightarrow g(\bar{p}_1, \bar{\lambda}_1)g(\bar{p}_2, \bar{\lambda}_2)\gamma(\bar{p}_3, \bar{\lambda}_3)\gamma(\bar{p}_4, \bar{\lambda}_4)g(\bar{p}_5, \bar{\lambda}_5)$. The momenta \bar{p}_i and helicities $\bar{\lambda}_i$ are related to the physical momenta p_i and helicities λ_i as $\{\bar{p}_i, \bar{\lambda}_i\} = \{-p_i, -\lambda_i\}$ for $i = 1$ or 2 , and $\{\bar{p}_i, \bar{\lambda}_i\} = \{p_i, \lambda_i\}$ for $i = 3, 4$, or 5 . $\mathcal{M}_5(1, 2, 3, 4, 5)$ is a shorthand notation for $\mathcal{M}_5(\bar{p}_1, \bar{\lambda}_1; \bar{p}_2, \bar{\lambda}_2; \bar{p}_3, \bar{\lambda}_3; \bar{p}_4, \bar{\lambda}_4; \bar{p}_5, \bar{\lambda}_5)$.

The amplitude $\mathcal{M}_5(1, 2, 3, 4, 5)$ was derived in Refs. [20, 21] from color-decomposed 5-gluon 1-loop scattering amplitudes [9]. $\mathcal{M}_5(1, 2, 3, 4, 5)$ is built from 1-loop partial amplitudes $A_{5;1}(1, 2, 3, 4, 5)$ for the $0 \rightarrow gg\gamma\gamma g$ scattering process, identical to the partial amplitudes for $0 \rightarrow ggggg$ scattering via a spin-1/2 fermion loop [9]. The squared 5-leg amplitude, averaged over spins, colors, and identical final-state particles, is

$$|\mathcal{M}_5|^2 = \sigma_g^{(1)} \sum_{\bar{\lambda}_1, \bar{\lambda}_2, \bar{\lambda}_3, \bar{\lambda}_4, \bar{\lambda}_5} \left| \sum_{\sigma \in \text{COP}_3^{(125)}} A_{5;1}(\sigma_1, \sigma_2, \sigma_3, \sigma_4, \sigma_5) \right|^2, \quad (\text{B2})$$

with

$$\sigma_g^{(1)} \equiv (4\pi)^5 \alpha_s^3 \alpha^2 \left(\sum_i e_i^2 \right)^2 \frac{N_c}{N_c^2 - 1}. \quad (\text{B3})$$

The partial amplitudes are summed over all permutations σ of the external indices (1,2,3,5) with a fixed cyclic ordering of (1,2,5), i.e., cyclically-ordered (COP) permutations:

$$\begin{aligned} \sum_{\sigma \in \text{COP}_3^{(125)}} A_{5;1}(\sigma_1, \sigma_2, \sigma_3, \sigma_4, \sigma_5) \equiv & \\ & A_{5;1}(1, 2, 5, 3, 4) + A_{5;1}(1, 2, 3, 5, 4) + A_{5;1}(1, 3, 2, 5, 4) + A_{5;1}(3, 1, 2, 5, 4) + \\ & A_{5;1}(5, 1, 2, 3, 4) + A_{5;1}(5, 1, 3, 2, 4) + A_{5;1}(5, 3, 1, 2, 4) + A_{5;1}(3, 5, 1, 2, 4) + \\ & A_{5;1}(2, 5, 1, 3, 4) + A_{5;1}(2, 5, 3, 1, 4) + A_{5;1}(2, 3, 5, 1, 4) + A_{5;1}(3, 2, 5, 1, 4). \end{aligned} \quad (\text{B4})$$

The collinear and soft behaviors of the amplitude \mathcal{M}_5 can be established by following the approach in Refs. [8, 9, 10, 11, 12, 13, 14], extended recently to the two-loop level [59, 60]. When gluon 5 is collinear to gluon 1, the amplitude $\mathcal{M}_5(1, 2, 3, 4, 5)$ is dominated by six partial amplitudes with cyclically adjacent indices 5 and 1, such as $A_{5;1}(5, 1, 2, 3, 4)$. Similarly, when gluon 5 is collinear to gluon 2, $\mathcal{M}_5(1, 2, 3, 4, 5)$ is dominated by six partial amplitudes with cyclically adjacent indices 2 and 5. Each leading partial amplitude $A_{5;1}(\dots, 5, 1, \dots)$ factors in the $5 \parallel 1$ collinear limit into a 4-leg partial amplitude $A_{4;1}(\dots, I, \dots)$ for production of 2, 3, 4, and intermediate gluon I , and amplitude $\text{Split}_{-\bar{\lambda}_I}^{tree}(5, 1)$ [61, 62, 63, 64] describing tree-level splitting of I into 5 and 1:

$$A_{5;1}(\dots, 5, 1, \dots) \xrightarrow{5 \parallel 1} \sum_{\bar{\lambda}_I = \pm 1} \text{Split}_{-\bar{\lambda}_I}^{tree}(5, 1) A_{4;1}(\dots, I, \dots) + \text{subleading terms}. \quad (\text{B5})$$

The ellipses in Eq. (B5) denote the same permutation of indices 2, 3, and 4 in $A_{5;1}$ and $A_{4;1}$. The amplitudes $\text{Split}_{-\bar{\lambda}_I}^{tree}(5, 1)$ are universal functions of the momenta \bar{p}_I , \bar{p}_1 , and \bar{p}_5 , which in our case satisfy $\bar{p}_I \equiv \bar{p}_1 + \bar{p}_5$, $\bar{p}_1 = (1 - z)\bar{p}_I$, and $\bar{p}_5 = z\bar{p}_I$, where $z = 1 - 1/\hat{x}_1$. The right-hand side of Eq. (B5) is summed over the helicities $\bar{\lambda}_I$ of I . The collinear factorization

relation applies to any one-loop n -leg primitive amplitude $A_n^{loop}(1, \dots, n)$:

$$A_n^{loop}(\dots, a, b, \dots) \xrightarrow{a||b} \sum_{\bar{\lambda}_I} \left[\text{Split}_{-\bar{\lambda}_I}^{tree}(a, b) A_{n-1}^{loop}(\dots, I, \dots) + \text{Split}_{-\bar{\lambda}_I}^{loop}(a, b) A_{n-1}^{tree}(\dots, I, \dots) \right] \quad (\text{B6})$$

Equation (B6) is evaluated here for $n = 5$ external legs, along with the condition that the tree primitive amplitude A_4^{tree} vanishes in $0 \rightarrow gg\gamma\gamma$ process.

Using Eqs. (B2), (B4), (B5), we derive the approximate form for $|\mathcal{M}_5|^2$ in the $5 \parallel 1$ limit:

$$|\mathcal{M}_5(1, 2, 3, 4, 5)|^2 \xrightarrow{5||1} \sigma_g^{(1)} \sum_{\bar{\lambda}_I, \bar{\lambda}'_I = \pm 1} \mathcal{M}_4^*(\bar{p}_I, \bar{\lambda}'_I; 2, 3, 4) T_{\bar{\lambda}'_I, \bar{\lambda}_I}(\hat{x}_1) \mathcal{M}_4(\bar{p}_I, \bar{\lambda}_I; 2, 3, 4). \quad (\text{B7})$$

Here $\mathcal{M}_4(I, 2, 3, 4) \equiv \sum_{\sigma \in S_3} A_{4;1}(I, \sigma_2, \sigma_3, \sigma_4)$ is the normalized 4-leg amplitude, obtained by summation of the partial amplitudes $A_{4;1}(I, 2, 3, 4)$ over all possible permutations S_3 of the legs 2, 3, and 4. The amplitude \mathcal{M}_4 and complex-conjugate amplitude \mathcal{M}_4^* are evaluated for independent helicities $\bar{\lambda}_I$ and $\bar{\lambda}'_I$ of I . $T_{\bar{\lambda}'_I, \bar{\lambda}_I}(\hat{x}_1)$ absorbs contributions from the splitting amplitudes:

$$T_{\bar{\lambda}_I, \bar{\lambda}'_I}(\hat{x}_1) \equiv \sum_{\bar{\lambda}_1, \bar{\lambda}_5 = \pm 1} \left[\text{Split}_{-\bar{\lambda}_I}^{tree}\left(\frac{1}{\hat{x}_1}; 1, 5\right) \right]^* \text{Split}_{-\bar{\lambda}'_I}^{tree}\left(\frac{1}{\hat{x}_1}; 1, 5\right). \quad (\text{B8})$$

In a basis with $\bar{\lambda} = +1$ and $\bar{\lambda} = -1$, $T_{\bar{\lambda}'_I, \bar{\lambda}_I}(x)$ is a matrix of the form

$$T_{\bar{\lambda}'_I, \bar{\lambda}_I}(x) = \frac{2C_A}{2xp_1 \cdot p_5} \begin{pmatrix} \frac{x}{1-x} + \frac{1-x}{x} + x(1-x) & -\frac{1-x}{x} \frac{[51]}{[51]} \\ -\frac{1-x}{x} \frac{\langle 51 \rangle}{[51]} & \frac{x}{1-x} + \frac{1-x}{x} + x(1-x) \end{pmatrix}. \quad (\text{B9})$$

The diagonal entries of $T_{\bar{\lambda}'_I, \bar{\lambda}_I}(\hat{x}_1)$ give rise to terms proportional to the unpolarized splitting function $P_{g/g}(\hat{x}_1)$ in the asymptotic cross section, with

$$P_{g/g}(\hat{x}_1) = 2C_A \left[\frac{\hat{x}_1}{(1-\hat{x}_1)_+} + \frac{1-\hat{x}_1}{\hat{x}_1} + \hat{x}_1(1-\hat{x}_1) \right] + \frac{11N_c - 2N_f}{6} \delta(1-\hat{x}_1), \quad (\text{B10})$$

where N_f is the number of active quark flavors. The off-diagonal entries give rise to terms proportional to the spin-flip splitting function

$$P'_{g/g}(\hat{x}_1) = 2C_A(1-\hat{x}_1)/\hat{x}_1, \quad (\text{B11})$$

multiplied by the ratio of spinor products $\langle 51 \rangle \equiv \langle 5 + |1 - \rangle$ and $[51] \equiv \langle 5 - |1 + \rangle$. In a general reference frame, $\langle 51 \rangle/[51]$ is a complex phase depending on the azimuthal separation $\varphi_1 - \varphi_5$ between the gluons 1 and 5. In the Collins-Soper frame, this phase reduces to $\langle 51 \rangle/[51] = -1$.²

² A collinear approximation for $|\mathcal{M}_5|^2$ is derived in Ref. [23] in the framework of the dipole factorization formalism [25]. This approximation agrees with ours up to phases of the off-diagonal terms, which are not the same as in Eq. (B9). Our expression is shown upon a closer examination to produce correct phases in an arbitrary reference frame [65].

Next, we employ explicit expressions for $\mathcal{M}_4(I, 2, 3, 4)$ from Ref. [22], given by products $\mathcal{M}_4(I, 2, 3, 4) = S_{\bar{\lambda}_I \bar{\lambda}_2 \bar{\lambda}_3 \bar{\lambda}_4} M_{\bar{\lambda}_I \bar{\lambda}_2 \bar{\lambda}_3 \bar{\lambda}_4}^{(1)}$ of reduced matrix elements $M_{\bar{\lambda}_I \bar{\lambda}_2 \bar{\lambda}_3 \bar{\lambda}_4}^{(1)}$ and phase factors $S_{\bar{\lambda}_I \bar{\lambda}_2 \bar{\lambda}_3 \bar{\lambda}_4}$. With these expressions inserted, Eq. (B7) becomes in the Collins-Soper frame

$$|\mathcal{M}_5(1, 2, 3, 4, 5)|^2 \xrightarrow{5||1} \frac{\sigma_g^{(1)}}{2\hat{x}_1 p_1 \cdot p_5} \left\{ P_{g/g}(\hat{x}_1) L_g(\theta_*) + P'_{g/g}(\hat{x}_1) L'_g(\theta_*) \cos 2\varphi_* \right\}, \quad (\text{B12})$$

where

$$L_g(\theta_*) = \sum_{\bar{\lambda}_1, \bar{\lambda}_2, \bar{\lambda}_3, \bar{\lambda}_4} \left| M_{\bar{\lambda}_1 \bar{\lambda}_2 \bar{\lambda}_3 \bar{\lambda}_4}^{(1)} \right|^2, \quad (\text{B13})$$

and

$$L'_g(\theta_*) = -4\text{Re} \left\{ M_{1,1,-1,-1}^{(1)} + M_{1,-1,1,-1}^{(1)} + M_{-1,1,1,-1}^{(1)} + 1 \right\}. \quad (\text{B14})$$

In the $5 \parallel 2$ collinear limit $|\mathcal{M}_5|^2$ is

$$|\mathcal{M}_5(1, 2, 3, 4, 5)|^2 \xrightarrow{5||2} \frac{\sigma_g^{(1)}}{2\hat{x}_2 p_2 \cdot p_5} \left\{ P_{g/g}(\hat{x}_2) L_g(\theta_*) + P'_{g/g}(\hat{x}_2) L'_g(\theta_*) \cos 2\varphi_* \right\}. \quad (\text{B15})$$

In the soft limit $p_5^\mu \rightarrow 0$, $|\mathcal{M}_5|^2$ factors as

$$|\mathcal{M}_5(1, 2, 3, 4, 5)|^2 \rightarrow \frac{1}{Q_T^2} 2C_A \frac{\alpha_s}{\pi} |\mathcal{M}_4(1, 2, 3, 4)|^2 + \text{subleading terms}. \quad (\text{B16})$$

Inserting collinear and soft approximations (B12), (B15), and (B16) in Eq. (B1) and making some simplifications, we derive the asymptotic expression for real-emission contributions,

$$\begin{aligned} & \left. \frac{d\sigma_{gg}}{dQ^2 dy dQ_T^2 d\Omega_*} \right|_{\text{real}} \rightarrow \frac{\sigma_g^{(0)}}{S} \frac{1}{2\pi Q_T^2} \frac{\alpha_s}{\pi} \\ & \times \left\{ L_g(\theta_*) \left(f_{g/h_1}(x_1, \mu_F) f_{g/h_2}(x_2, \mu_F) \left(\mathcal{A}_g^{(1,c)} \ln \frac{Q^2}{Q_T^2} + \mathcal{B}_g^{(1,c)} \right) \right. \right. \\ & + \left[P_{g/g} \otimes f_{g/h_1} \right] (x_1, \mu_F) f_{g/h_2}(x_2, \mu_F) + f_{g/h_1}(x_1, \mu_F) \left[P_{g/g} \otimes f_{g/h_2} \right] (x_2, \mu_F) \\ & + \cos 2\varphi_* L'_g(\theta_*) \left(\left[P'_{g/g} \otimes f_{g/h_1} \right] (x_1, \mu_F) f_{g/h_2}(x_2, \mu_F) \right. \\ & \left. \left. + f_{g/h_1}(x_1, \mu_F) \left[P'_{g/g} \otimes f_{g/h_2} \right] (x_2, \mu_F) \right) \right\}. \quad (\text{B17}) \end{aligned}$$

Once we add the two-loop 4-leg virtual corrections [Fig. 1(e)], the soft singularities in the real-emission cross section residing at $Q_T = 0$ are canceled [23, 43]. The final small- Q_T expression coincides with Eq. (16).

[1] J. C. Collins, D. E. Soper, and G. Sterman, Nucl. Phys. **B250**, 199 (1985).

[2] ATLAS Collaboration, *ATLAS detector and physics performance. Technical design report. Vol. 2* (1999), CERN-LHCC-99-15.

- [3] CMS Collaboration, *CMS physics. Technical design report. Vol. 2* (2006), CERN-LHCC 2006-021.
- [4] S. Abdullin et al., *Eur. Phys. J.* **C39S2**, 41 (2005).
- [5] C. Balazs, E. L. Berger, P. Nadolsky, and C. P. Yuan, *Phys. Lett.* **B637**, 235 (2006).
- [6] C. Balazs, E. L. Berger, P. M. Nadolsky, and C. P. Yuan (2007), arXiv:0704.0001 [hep-ph].
- [7] C. Balazs, E. L. Berger, S. Mrenna, and C.-P. Yuan, *Phys. Rev.* **D57**, 6934 (1998).
- [8] Z. Bern, L. J. Dixon, and D. A. Kosower, *Nucl. Phys.* **B437**, 259 (1995).
- [9] Z. Bern, L. J. Dixon, and D. A. Kosower, *Phys. Rev. Lett.* **70**, 2677 (1993).
- [10] Z. Bern, G. Chalmers, L. J. Dixon, and D. A. Kosower, *Phys. Rev. Lett.* **72**, 2134 (1994).
- [11] Z. Bern, L. J. Dixon, D. C. Dunbar, and D. A. Kosower, *Nucl. Phys.* **B425**, 217 (1994).
- [12] Z. Bern, V. Del Duca, and C. R. Schmidt, *Phys. Lett.* **B445**, 168 (1998).
- [13] Z. Bern, V. Del Duca, W. B. Kilgore, and C. R. Schmidt, *Phys. Rev.* **D60**, 116001 (1999).
- [14] D. A. Kosower and P. Uwer, *Nucl. Phys.* **B563**, 477 (1999).
- [15] J. C. Collins and D. E. Soper, *Phys. Rev.* **D16**, 2219 (1977).
- [16] P. Aurenche, A. Douiri, R. Baier, M. Fontannaz, and D. Schiff, *Z. Phys.* **C29**, 459 (1985).
- [17] B. Bailey, J. F. Owens, and J. Ohnemus, *Phys. Rev.* **D46**, 2018 (1992).
- [18] T. Binoth, J. P. Guillet, E. Pilon, and M. Werlen, *Eur. Phys. J.* **C16**, 311 (2000).
- [19] E. L. Berger, E. Braaten, and R. D. Field, *Nucl. Phys.* **B239**, 52 (1984).
- [20] C. Balazs, P. Nadolsky, C. Schmidt, and C.-P. Yuan, *Phys. Lett.* **B489**, 157 (2000).
- [21] D. de Florian and Z. Kunszt, *Phys. Lett.* **B460**, 184 (1999).
- [22] Z. Bern, A. De Freitas, and L. J. Dixon, *JHEP* **09**, 037 (2001).
- [23] Z. Bern, L. J. Dixon, and C. Schmidt, *Phys. Rev.* **D66**, 074018 (2002).
- [24] Y. Yasui, *Phys. Rev.* **D66**, 094012 (2002).
- [25] S. Catani and M. H. Seymour, *Nucl. Phys.* **B485**, 291 (1997).
- [26] J. C. Collins and D. E. Soper, *Nucl. Phys.* **B193**, 381 (1981).
- [27] J. C. Collins and D. E. Soper, *Nucl. Phys.* **B197**, 446 (1982).
- [28] J. P. Ralston and D. E. Soper, *Nucl. Phys.* **B152**, 109 (1979).
- [29] D. E. Soper, *Phys. Rev.* **D15**, 1141 (1977).
- [30] D. E. Soper, *Phys. Rev. Lett.* **43**, 1847 (1979).
- [31] R. Ali and P. Hoodbhoy, *Z. Phys.* **C57**, 325 (1993).
- [32] S. V. Bashinsky and R. L. Jaffe, *Nucl. Phys.* **B536**, 303 (1998).
- [33] J. C. Collins and D. E. Soper, *Nucl. Phys.* **B194**, 445 (1982).
- [34] P. J. Mulders and J. Rodrigues, *Phys. Rev.* **D63**, 094021 (2001), and references therein.
- [35] Y. L. Dokshitzer, *Sov. Phys. JETP* **46**, 641 (1977).
- [36] V. N. Gribov and L. N. Lipatov, *Sov. J. Nucl. Phys.* **15**, 438 (1972).
- [37] V. N. Gribov and L. N. Lipatov, *Sov. J. Nucl. Phys.* **15**, 675 (1972).
- [38] G. Altarelli and G. Parisi, *Nucl. Phys.* **B126**, 298 (1977).
- [39] R. D. Tangerman and P. J. Mulders, *Phys. Rev.* **D51**, 3357 (1995), and references therein.
- [40] A. A. Henneman, D. Boer, and P. J. Mulders, *Nucl. Phys.* **B620**, 331 (2002).
- [41] D. Boer, *Nucl. Phys.* **B603**, 195 (2001).
- [42] A. Idilbi, X. Ji, J.-P. Ma, and F. Yuan, *Phys. Rev.* **D70**, 074021 (2004).
- [43] P. M. Nadolsky and C. R. Schmidt, *Phys. Lett.* **B558**, 63 (2003).
- [44] C.-P. Yuan, *Phys. Lett.* **B283**, 395 (1992).
- [45] A. Vogt, S. Moch, and J. A. M. Vermaseren, *Nucl. Phys.* **B691**, 129 (2004).
- [46] C. Balazs and C.-P. Yuan, *Phys. Rev.* **D56**, 5558 (1997).
- [47] S. Catani, D. de Florian, and M. Grazzini, *Nucl. Phys.* **B596**, 299 (2001).

- [48] E. L. Berger and J. Qiu, Phys. Rev. **D67**, 034026 (2003).
- [49] A. V. Konychev and P. M. Nadolsky, Phys. Lett. **B633**, 710 (2006).
- [50] F. Landry, R. Brock, P. M. Nadolsky, and C.-P. Yuan, Phys. Rev. **D67**, 073016 (2003).
- [51] G. A. Ladinsky and C.-P. Yuan, Phys. Rev. **D50**, 4239 (1994).
- [52] C. Balazs (1999), hep-ph/9906422.
- [53] D. Acosta et al. (CDF Collaboration), Phys. Rev. Lett. **95**, 022003 (2005).
- [54] R. V. Harlander and W. B. Kilgore, Phys. Rev. Lett. **88**, 201801 (2002).
- [55] C. Anastasiou, K. Melnikov, and F. Petriello, Phys. Rev. Lett. **93**, 262002 (2004).
- [56] C. Anastasiou, K. Melnikov, and F. Petriello, Nucl. Phys. **B724**, 197 (2005).
- [57] S. Berge, P. Nadolsky, F. Olness, and C.-P. Yuan, Phys. Rev. **D72**, 033015 (2005).
- [58] D. Binosi and L. Theussl, Comput. Phys. Commun. **161**, 76 (2004).
- [59] Z. Bern, L. J. Dixon, and D. A. Kosower, JHEP **08**, 012 (2004).
- [60] S. D. Badger and E. W. N. Glover, JHEP **07**, 040 (2004).
- [61] S. J. Parke and T. R. Taylor, Phys. Rev. Lett. **56**, 2459 (1986).
- [62] M. L. Mangano and S. J. Parke, Nucl. Phys. **B299**, 673 (1988).
- [63] F. A. Berends and W. T. Giele, Nucl. Phys. **B306**, 759 (1988).
- [64] M. L. Mangano and S. J. Parke, Phys. Rept. **200**, 301 (1991).
- [65] L. Dixon, private communication.
- [66] D. de Florian and M. Grazzini, Phys. Rev. Lett. **85**, 4678 (2000).
- [67] S. Moch, J. A. M. Vermaseren, and A. Vogt, Nucl. Phys. **B688**, 101 (2004).